

Comparing Effective One Body Hamiltonians for spin-aligned coalescing binaries

Piero Rettegno^{1,2}, Fabio Martinetti^{1,2}, Alessandro Nagar^{1,3}, Donato Bini^{4,5}, Gunnar Riemenschneider^{1,2}, and Thibault Damour³

¹*INFN Sezione di Torino, Via P. Giuria 1, 10125 Torino, Italy*

²*Dipartimento di Fisica, Università di Torino, via P. Giuria 1, 10125 Torino, Italy*

³*Institut des Hautes Etudes Scientifiques, 91440 Bures-sur-Yvette, France*

⁴*Istituto per le Applicazioni del Calcolo “M. Picone”, CNR, I-00185 Rome, Italy and*

⁵*INFN, Sezione di Roma Tre, I-00146 Roma, Italy*

TEOBResumS and SEOBNRv4 are the two existing semi-analytical gravitational waveform models for spin-aligned coalescing black hole binaries based on the effective-one-body approach. They are informed by numerical relativity simulations and provide the relative dynamics and waveforms from early inspiral to plunge, merger and ringdown. The central building block of each model is the EOB resummed Hamiltonian. The two models implement different Hamiltonians that are both deformations of the Hamiltonian of a test spinning black hole moving around a Kerr black hole. Here we analytically compare, element by element, the two Hamiltonians. In particular: we illustrate that one can introduce a *centrifugal radius* in SEOBNRv4, so to rewrite the Hamiltonian in a more compact form that is analogous to the one of TEOBResumS. The latter centrifugal radius cannot, however, be identified with the one used in TEOBResumS because the two models differ in their ways of incorporating spin effects in their respective deformations of the background Kerr Hamiltonian. We performed extensive comparisons between the energetics corresponding to the two Hamiltonians using gauge-invariant quantities. Finally, as an exploratory investigation, we apply the post-adiabatic approximation to the newly rewritten SEOBNRv4 Hamiltonian, illustrating that it is possible to generate long-inspiral waveforms with negligible computational cost.

I. INTRODUCTION

Gravitational wave (GW) astronomy with coalescing compact binaries (CBC), either binary neutron stars (BNS) or binary black holes (BBH), needs accurate waveform modeling. Efficient and accurate, analytical, waveform models were essential for the analysis of the so-far published 11 GW transients (10 BBHs and 1 BNS [1]) discovered by the LIGO and Virgo collaboration. The effective-one-body (EOB) approach to the general relativistic two-body problem [2–5] represents one of the most complete, accurate and flexible analytical formalism able to describe the binary dynamics and waveform from coalescing compact binaries from the early inspiral, through plunge, merger, postmerger and ringdown. The crucial improvement brought by the EOB formalism is that it *resums*, in special ways, state-of-the-art post-Newtonian (PN) results [6, 7] so to improve their predictive power and robustness in the strong-field, fast-velocity regime. Once complemented by strong-field, non-perturbative, information provided by Numerical Relativity (NR) simulations to improve the behavior of the EOB dynamics and waveform in the last few orbits (as well as in the merger-ringdown phase) one has access to EOB-NR theoretical waveform models, routinely used on GW transient data by the LIGO-Virgo collaboration. The construction of such models has been a long process, with progressive steps forward related to both: (i) new theoretical ideas and developments and (ii) the improved accuracy of NR simulations. Nowadays, SEOBNRv4 [8], SEOBNRv4HM [9] (its version with higher modes) and TEOBResumS [10, 11] are the two state-of-the-art EOB models, improved (or calibrated) by NR simulations for spin-aligned compact binaries. For generic, precessing, spins currently only the SEOBNRv3 model is available [12, 13], while SEOBNRv4PHM (that incorporates both higher modes and precession effects) is in progress [14]. The model TEOBResumS also incorporates matter effects [that is, tidal interactions

as well as EOS dependent spin-square effects [11] up to next-to-next-to-leading order (NNLO)] so to provide BNS waveforms and has been recently extended to also have a phenomenological description of the BNS post-merger phase [15]. By contrast SEOBNRv4T [16–18] is the tidal extension of SEOBNRv4 that incorporates “dynamical tides” [17], that is a special enhancement of the tidal interaction due to the coupling between the orbital motion and the f -mode oscillation of each neutron star.

The EOB model is characterized by three building blocks: (i) a Hamiltonian that describes the conservative part of the relative dynamics; (ii) a flux, that accounts for the energy and angular momentum losses through GW emission; (iii) a prescription for computing the waveform from this dynamics. Although SEOBNRv4 and TEOBResumS are *both* EOB-based waveform models and the waveform they provide are both considered “faithful”, by current standards, when compared to NR simulations, they were developed independently and are structurally different, especially for what concerns the conservative dynamics. The aim of this paper is to compare and contrast among the two Hamiltonians, so to highlight the analytical similarities and differences between them. For SEOBNRv4 we will condense here, and suitably rewrite, the information distributed in Refs. [8, 19–24]. For TEOBResumS we will refer to [10, 25–28]. Loosely speaking, an EOB Hamiltonian that describes the relative dynamics of a two-body system, with comparable masses (m_1, m_2), is always constructed as a *deformation* of the Hamiltonian of a (spinning) particle moving on a Schwarzschild (for nonspinning bodies) or Kerr (for spinning bodies) space-time. The deformation parameter is the symmetric mass ratio $\nu \equiv m_1 m_2 / (m_1 + m_2)^2$. There might be a certain degree of arbitrariness in this process, provided that two constraints are preserved: (i) on the one hand, one must recover the known, ν -dependent, PN results; (ii) on the other hand, one wants the exact test-particle Hamiltonian to be correctly recovered when $\nu \rightarrow 0$. Such process of de-

formation crucially regards also the spins. For example, starting from the Hamiltonian of a spinning particle on a rotating black hole (BH), there are several ways of defining “effective spins” that are combinations of the spins of two objects when the masses are comparable. In simple words, the main differences between the `TEOBResumS` and `SEOBNRv4` Hamiltonians is that the ν -deformation of the limiting Kerr one was implemented in different ways. In particular, the constructions of the two models were rooted in different ways of thinking about the extreme-mass-ratio limit ($m_2/m_1 \rightarrow 0$) of a system of two spinning BHs (see Sec. II below). This conceptual difference then entailed distinct approaches to defining the respective ν -deformations, with emphases on different parts of the spin-dependent dynamics, as well as different ways to incorporate the non-perturbative information extracted from NR simulations. As a consequence, one cannot define a one-to-one map between the various building blocks of the two EOB models. However, both models incorporate (modulo the choice of different gauges) the same PN information. On top of such structural difference, the two Hamiltonians also differ because of: (i) the choice of the effective-spin variable, which entails a different EOB representation of spin-spin effects, that are only partially resummed, already at leading order (LO), in `SEOBNRv4`; (ii) the spin-orbit sector, both because of the different ν -deformation and because of the contribution of the Hamiltonian of a spinning particle is only partially included in `TEOBResumS`, while it is fully incorporated in `SEOBNRv4`; (iii) the gauge choice for the spin-orbit sector of above; (iv) the resummation of the various potentials entering the Hamiltonian. To facilitate the comparison, we found that it is possible to modify the original notation of the `SEOBNRv4` Hamiltonian [19], by introducing a suitable, new, centrifugal radius function. This allows us to bring the structure of `SEOBNRv4` Hamiltonian much closer to the one of `TEOBResumS`, providing easier comparisons between the various functions.

The paper is organized as follows: in Sec. II we review the Hamiltonian of a spinning test-body (a particle) on a Kerr BH in equatorial motion, and introduce several useful analytic structures. In Sec. III we review the `TEOBResumS` Hamiltonian. The `SEOBNRv4` one is studied in Sec. IV, where various subsection are dedicated to a substantial rewriting of the expressions of Ref. [19] (specified to spin-aligned binaries) so to put them in a notation similar to the `TEOBResumS` one. In particular, Sec. IV A illustrates that a new centrifugal radius function can be introduced so that (part of) the even-in-spin sector can be recasted in a way formally analogous, though quantitatively different, to the corresponding one of `TEOBResumS`, see Eq. (64). Similarly, Sec. IV B performs a similar operation on the spin-orbit sector of the effective Hamiltonian and eventually illustrates that it is formally analogous to the one of `TEOBResumS`, though with different gyro-gravitomagnetic functions. Finally, Sec. IV C applies the same procedure also on the remaining part of the spin-spin contribution, that is written in compact form in Eq. (89). We also highlight, in the same section, how the LO spin-spin term is recovered from either model. Section V is dedicated to select comparisons between the energetics of the two Hamiltonians, so to especially point out differences in the spin-spin sector. We also analyse, in Sec. V C the

performance of a new nonspinning EOB model that is based on the `TEOBResumS` framework but where the A potential is resummed like in `SEOBNRv4`. Finally, to put our results in perspective for GW data analysis applications, in Sec. VI we construct a EOB model that uses the `SEOBNRv4` Hamiltonian, with a certain radiation reaction force and waveform, and apply to it the post-adiabatic approximation of Ref. [28] to solve the inspiral dynamics. This allows us to compute long-inspiral waveforms using the `SEOBNRv4` Hamiltonian, as previously done for `TEOBResumS` [11, 28, 29]. Throughout this work we use geometric units with $G = c = 1$.

II. HAMILTONIAN OF A SPINNING PARTICLE ON A KERR BACKGROUND

Both EOB models use as starting point the Hamiltonian of a test spinning object around a background spinning BH (described by a Kerr metric). However, the constructions of the two spinning EOB models were rooted in different ways of considering the extreme-mass-ratio ($m_2 \ll m_1$, i.e. $\nu \rightarrow 0$) limit defining the undeformed, background Kerr Hamiltonian. The `TEOBResumS` construction was initially based on Ref. [30] which considered the extreme-mass-ratio limit of a system of two spinning BHs, while the `SEOBNRv4` construction was initially based on Refs. [19–21], which considered the extreme-mass-ratio limit describing a test particle endowed with an *unlimited* spin moving in a Kerr metric. The difference between the two ways of considering the limit is that, as the spin of a small BH of mass $m_2 \ll m_1$ is physically bounded by the inequality $\chi_2 \leq 1$, i.e. $S_2 \leq m_2^2$, the former way of thinking about the limit leads to an Hamiltonian describing a nonspinning test particle around a Kerr BH. Technically, when considering the general Hamiltonian described in Eq.(22) below, the spin combination \hat{S}_* defined in Eq.(18) goes to zero proportionally to ν in this way of considering the extreme-mass-ratio limit. By contrast, in the second way of considering the extreme-mass-ratio limit, in which one formally considers overspinning test objects having $\chi_2 \gg 1$, but a fixed value of $\tilde{a}_2 = S_2/(m_2M)$, the spin combination \hat{S}_* does not go to zero as $\nu \rightarrow 0$. This motivated Ref.[19, 21] to pay particular attention to the part of the spin-orbit sector linked to the coupling of \hat{S}_* , i.e. to the second gyro-gravitomagnetic factor G_{S_*} in Eq.(38) below. On the other hand, the construction of the `TEOBResumS` model paid particular attention to the first gyro-gravitomagnetic factor G_S , and, following the construction of the first spinning EOB model [31], to ways of incorporating spin-spin effects through the definition of a suitable background Kerr spin variable \tilde{a}_0 (see below).

In this Section, we indicate with M the mass of the Kerr BH and with μ the mass of the particle. Their spins are addressed as S_{Kerr} and S_* respectively, with dimensionless spin variables that read $\hat{a} \equiv S_{\text{Kerr}}/M^2$ and $\tilde{a}_* \equiv S_*/(\mu M)$. We restrict ourselves to equatorial orbits ($\theta = \pi/2$) and parallel spins, using dimensionless phase space variables defined as ($r \equiv R/M$, $t \equiv T/M$, $p_r \equiv P_r/\mu$, $p_\varphi \equiv P_\varphi/(\mu M)$).

The Kerr metric in Boyer-Lindquist coordinates and re-

stricted to the equatorial plane reads

$$ds^2 = -\frac{\Lambda}{\Delta^K \Sigma} dt^2 + \frac{\Delta^K}{\Sigma} dr^2 + \frac{1}{\Lambda} \left(-\frac{4r^2 \hat{a}^2}{\Delta^K \Sigma} + \Sigma \right) d\varphi^2 - \frac{2r\hat{a}}{\Delta^K \Sigma} dt d\varphi, \quad (1)$$

where

$$\Sigma \equiv r^2, \quad (2)$$

$$\Delta^K \equiv r^2 \left(1 - \frac{2}{r} \right) + \hat{a}^2, \quad (3)$$

$$\Lambda \equiv (r^2 + \hat{a}^2)^2 - \hat{a}^2 \Delta^K. \quad (4)$$

From the relativistic mass-shell condition $g^{\mu\nu} p_\mu p_\nu = -1$, one obtains the Hamiltonian of a nonspinning particle on a Kerr background, $\hat{H}_0^K \equiv -p_0$, as

$$\hat{H}_0^K = \alpha \sqrt{1 + \gamma^{ij} p_i p_j} + \beta^i p_i, \quad (5)$$

with standard lapse-shift decomposition of the metric

$$\alpha = \frac{1}{\sqrt{-g^{tt}}}, \quad (6)$$

$$\beta^i = \frac{g^{ti}}{g^{tt}}, \quad (7)$$

$$\gamma^{ij} = g^{ij} - \frac{g^{ti} g^{tj}}{g^{tt}}. \quad (8)$$

The same Hamiltonian can be written equivalently as

$$\hat{H}_0^K = \sqrt{A^K \left(1 + \frac{p_\varphi^2}{(r_c^K)^2} + \frac{p_r^2}{B^K} \right)} + G_S^K \hat{a} p_\varphi, \quad (9)$$

where we introduced the centrifugal radius

$$(r_c^K)^2 = \frac{\Lambda}{\Sigma} = \frac{(r^2 + \hat{a}^2)^2 - \hat{a}^2 \Delta^K}{r^2} = r^2 + \hat{a}^2 \left(1 + \frac{2}{r} \right), \quad (10)$$

and the functions (A^K, B^K, r_c^K, G_S^K) are expressed in terms of the Kerr metric functions as

$$A^K = \frac{\Delta^K \Sigma}{\Lambda} = (1 - 2u_c^K) \frac{1 + 2u_c^K}{1 + 2u}, \quad (11)$$

$$B^K = \frac{\Sigma}{\Delta^K} = \frac{(u_c^K)^2}{u^2} \frac{1}{A^K}, \quad (12)$$

$$G_S^K = \frac{2r\hat{a}}{\Lambda} = 2u (u_c^K)^2, \quad (13)$$

where $u_c^K \equiv 1/r_c^K$. These two different formulations of the Kerr Hamiltonian are at the core of the differences between the two EOB-NR models dynamics. We will expand our discussion on this topic in the following sections.

When we consider a (over)spinning particle, an additional spin-orbit coupling term $G_{S_*}^K \tilde{a}_* p_\varphi$ is present, so that the Kerr Hamiltonian in the extreme mass-ratio limit [20, 25] reads

$$\hat{H}^K = \sqrt{A^K \left(1 + \frac{p_\varphi^2}{(r_c^K)^2} + \frac{p_r^2}{B^K} \right)} + (G_S^K \hat{a} + G_{S_*}^K \tilde{a}_*) p_\varphi. \quad (14)$$

The expression of $G_{S_*}^K$ is not trivial (see Ref. [19]). The re-derivation of Ref. [32] showed that for the equatorial, parallel-spin, case it can be written as (see Eq. (2.21) therein)

$$G_{S_*}^K = \frac{1}{(r_c^K)^2} \left\{ \frac{\sqrt{A^K}}{\sqrt{Q^K}} \left[1 - \frac{(r_c^K)'}{\sqrt{B^K}} \right] + \frac{r_c^K}{2(1 + \sqrt{Q^K})} \frac{(A^K)'}{\sqrt{A^K B^K}} \right\}, \quad (15)$$

where the radial derivatives are indicated as $(\cdot)' \equiv \partial_r(\cdot)$ and

$$Q^K \equiv 1 + \gamma^{ij} p_i p_j = 1 + p_\varphi^2 (u_c^K)^2 + \frac{p_r^2}{B^K}. \quad (16)$$

One can check that Eq. (15) is consistent with Eq. (3.18) Ref. [19] once specified to equatorial orbits.

III. THE HAMILTONIAN OF TEOBRESUMS

In the following, we will consider a binary system with masses m_i and spin vectors \mathbf{S}_i , with $i = 1, 2$. The projections of the spins along the direction of the orbital angular momentum are denoted by $S_i \equiv \mathbf{L} \cdot \mathbf{S}_i$. We denote the total mass by $M \equiv m_1 + m_2$ and the reduced mass as $\mu \equiv (m_1 m_2)/M$. We adopt the convention that $m_1 \geq m_2$. We hence define the mass ratio $q = m_1/m_2 \geq 1$ and symmetric mass ratio $\nu \equiv \mu/M = (m_1 m_2)/(m_1 + m_2)^2$. The mass fractions are expressed as $X_i \equiv m_i/M$. The dimensionless spin variables we use are $\chi_i \equiv S_i/m_i^2$ and $\tilde{a}_i \equiv S_i/(m_i M) = X_i \chi_i$, together with their combinations

$$\hat{S} \equiv \frac{S_1 + S_2}{M^2}, \quad (17)$$

$$\hat{S}_* \equiv \frac{1}{M^2} \left(\frac{m_2}{m_1} S_1 + \frac{m_1}{m_2} S_2 \right), \quad (18)$$

and

$$\tilde{a}_0 \equiv \tilde{a}_1 + \tilde{a}_2 = \hat{S} + \hat{S}_*, \quad (19)$$

$$\tilde{a}_{12} \equiv \tilde{a}_1 - \tilde{a}_2 = \frac{\hat{S} - \hat{S}_*}{X_{12}}, \quad (20)$$

where $X_{12} \equiv X_1 - X_2$. Like the case of a spinning particle on Kerr seen above, for spin-aligned binaries the four-dimensional phase space is described by $(\varphi, P_\varphi, R, P_{R_*})$ where φ is the orbital phase, P_φ the orbital angular momentum, R the radial separation and $P_{R_*} \equiv \sqrt{A/B} P_R$ the conjugate radial momentum with respect to the tortoise radial coordinate. Dimensionless phase space variables are $r \equiv R/M$, $p_{r_*} \equiv P_{R_*}/\mu$ and $p_\varphi \equiv P_\varphi/(\mu M)$, while dimensionless time is denoted as $t \equiv T/M$.

The TEOBResumS model [10] stems from the (equatorial) Hamiltonian introduced in Ref. [25]. An important element of the latter is the centrifugal radius that is used to incorporate, in a resummed way, spin-spin effects within the Hamiltonian. The EOB Hamiltonian reads

$$\hat{H}_{\text{EOB}} \equiv \frac{H_{\text{EOB}}}{\mu} = \frac{1}{\nu} \sqrt{1 + 2\nu (\hat{H}_{\text{eff}} - 1)}. \quad (21)$$

The effective Hamiltonian $\hat{H}_{\text{eff}} \equiv H_{\text{eff}}/\mu$ is constructed so as to closely mimic the structure of the (spinning) test-particle one described in Eq. (14) and is written as

$$\hat{H}_{\text{eff}} = \hat{H}_{\text{eff}}^{\text{orb}} + \left(G_S \hat{S} + G_{S_*} \hat{S}_* \right) p_\varphi, \quad (22)$$

where \hat{S} and \hat{S}_* reduce to the spin of the primary object and of the particle respectively when $m_1 \gg m_2$.

A. Orbital Hamiltonian

The orbital effective Hamiltonian in Eq. (22) reads

$$\hat{H}_{\text{orb}}^{\text{eff}} = \sqrt{A \left(1 + \frac{p_\varphi^2}{r_c^2} + 2\nu(4-3\nu) \frac{p_{r_*}^4}{r_c^2} \right) + p_{r_*}^2}, \quad (23)$$

where r_c is the EOB centrifugal radius that takes into account spin-spin interactions (see below) and the A function is written as

$$A = A_{\text{orb}}(u_c) \frac{1+2u_c}{1+2u}, \quad (24)$$

where

$$A_{\text{orb}}(u_c) = P_5^1 [A_{\text{orb}}^{5\text{PN}}](u_c), \quad (25)$$

is the orbital potential resummed with a (1,5) Padé approximant. The PN expanded orbital potential, at 5PN formal accuracy, reads

$$A_{\text{orb}}^{\text{PN}}(u) = 1 - 2u + 2\nu u^3 + \left(\frac{94}{3} - \frac{41\pi^2}{32} \right) \nu u^4 + \left(a_5^c + a_5^{\log} \log u \right) u^5 + \nu \left(a_6^c + a_6^{\log} \log u \right) u^6. \quad (26)$$

The 4PN and the logarithmic 5PN term are analytically known,

$$a_5^c = \left(\frac{2275\pi^2}{512} - \frac{4237}{60} + \frac{128}{5} \gamma_E + \frac{256}{5} \log 2 \right) \nu + \left(\frac{41\pi^2}{32} - \frac{221}{6} \right) \nu^2, \\ a_5^{\log} = \frac{64}{5} \nu, \\ a_6^{\log} = -\frac{7004}{105} \nu - \frac{144}{5} \nu^2, \quad (27)$$

where $\gamma_E = 0.57721\dots$ is Euler's constant and the (effective) 5PN term a_6^c is informed by NR simulations [10, 26, 27] (see Sec. III C below).

All terms proportional to even powers of the spins are incorporated in the EOB centrifugal radius r_c . This function is understood as a *deformation* of the Kerr one, Eq. (10), which reads

$$r_c^2 \equiv r^2 + \tilde{a}_0^2 \left(1 + \frac{2}{r} \right) + \frac{\delta a^2}{r}, \quad (28)$$

where the dimensionless Kerr spin is replaced by the dimensionless effective spin \tilde{a}_0 . The function $\delta \tilde{a}^2$ is introduced here to incorporate spin-spin terms beyond LO. The

BBH sector of **TEOBResumS** only includes next-to-leading order (NLO) spin-spin terms, so that this function explicitly reads [11]

$$\delta a^2 \equiv -\frac{1}{8} \left\{ 9\tilde{a}_0^2 + (1+4\nu)\tilde{a}_{12}^2 - 10X_{12}\tilde{a}_0\tilde{a}_{12} \right\}. \quad (29)$$

The other metric potential B is obtained through the D function, whose PN expression is

$$D_{\text{orb}}^{\text{PN}}(u) = 1 - 6\nu u^2 - 2(26-3\nu)\nu u^3. \quad (30)$$

Within **TEOBResumS**, this is resummed as

$$D \equiv AB = \frac{r^2}{r_c^2} D_{\text{orb}}(u_c), \quad (31)$$

with

$$D_{\text{orb}}(u_c) = P_3^0 [D_{\text{orb}}^{5\text{PN}}](u_c) \quad (32)$$

being the inverse resummation of its PN series.

B. Spin-orbit Hamiltonian

The spin-orbit contributions are encoded into the gyrogravitomagnetic functions (G_S, G_{S_*}) of Eq. (14). In **TEOBResumS** they are written in factorized form

$$G_S = G_S^0 \hat{G}_S, \quad (33)$$

$$G_{S_*} = G_{S_*}^0 \hat{G}_{S_*}, \quad (34)$$

where

$$G_{S_*}^0 = 2u u_c^2 \quad (35)$$

is the Kerr spin orbit coupling structure, in which r_c^K is replaced by the one defined in Eq. (28) above. $G_{S_*}^0$ is the leading PN correction (that can be also obtained by Taylor-expanding Eq. (15)) where u is replaced by u_c and reads

$$G_{S_*}^0 = \frac{3}{2} u_c^3. \quad (36)$$

In this respect, one should be reminded that Ref. [25] chose, for simplicity, to only use *part of* the analytical information encoded into the Hamiltonian of a spinning particle, Eq. (15), i.e. restricting it to the case of a Schwarzschild background and expanding it up to (next-to)³-leading order (N³LO). We stress this was a choice prompted both by the desire of constructing a rather simple model using the Damour-Jaranowski-Schäfer (DJS) gauge [30], where all dependence on the angular momentum p_φ is removed from (G_S, G_{S_*}), and by the idea that, in the physically relevant case of BBH systems, the G_{S_*} -type coupling is always secondary with respect to the G_S -type one because it contains an extra factor ν (with $\nu \leq 1/4$ in all cases). In the DJS gauge¹, the Hamiltonian of a spinning particle (either Schwarzschild or Kerr)

¹ The DJS gauge has the disadvantage of introducing formal (and fictitious [33]) singularities at the light ring, but it has many other useful properties: (i) it minimizes the effect of non-circularities during the late inspiral and the premerger phase; (ii) it allows, in principle, a clean separation between spin-orbit (odd in spin) and spin-spin (even in spin) effects.

becomes singular at light ring. So, the only way of incorporating some of this analytical information is by PN-expanding the corresponding G_{S_*} , that is then eventually resummed after in a different way. Note however that the *full* spinning-particle information can be incorporated also in a special flavor of **TEOBResumS**, notably in factorized form. To do so, however, a different spin gauge should be chosen. We shall briefly comment on this at the end of Sec. VII.

Finally, \hat{G}_S and \hat{G}_{S_*} are PN correcting factors that in **TEOBResumS** are inverse-resummed as

$$\hat{G}_S = (1 + c_{10}u_c + c_{20}u_c^2 + c_{30}u_c^3 + c_{02}p_{r^*}^2 + c_{12}u_cp_{r^*}^2 + c_{04}p_{r^*}^4)^{-1}, \quad (37)$$

$$\hat{G}_{S_*} = (1 + c_{10}^*u_c + c_{20}^*u_c^2 + c_{30}^*u_c^3 + c_{40}^*u_c^4 + c_{02}^*p_{r^*}^2 + c_{12}^*u_cp_{r^*}^2 + c_{04}^*p_{r^*}^4)^{-1}. \quad (38)$$

All coefficients are fully known analytically, with their complete ν dependence, except for (c_{30}^*, c_{40}^*) , which are those corresponding to the PN expansion of the spin-orbit sector of the Hamiltonian of a spinning particle on a Schwarzschild background [25]. In addition, the ν -dependence of c_{30} and c_{30}^* is informed by NR simulations. More precisely, we use $c_{30} \equiv \nu c_3$ and $c_{30}^* = 135/32 + \nu c_3$, where 135/32 is the spinning-particle value and c_3 is an NR-tuned effective N³LO parameter. The numerical values of the other coefficients in the DJS gauge are listed in Appendix B.

C. Numerical-relativity informed functions

The dynamics of **TEOBResumS** depends on two free functions (or flexibility parameters), a_6^c and c_3 , that are determined by comparison with NR simulations. The orbital Hamiltonian is NR-informed through a_6^c , that explicitly reads [10, 26, 27]

$$a_6^c = 3097.3 \nu^2 - 1330.6 \nu + 81.38. \quad (39)$$

The spin-orbit sector is instead calibrated using

$$c_3 = p_0 \frac{1 + n_1 \tilde{a}_0 + n_2 \tilde{a}_0^2}{1 + d_1 \tilde{a}_0} + (p_1 \nu + p_2 \nu^2 + p_3 \nu^3) \tilde{a}_0 X_{12} + p_4 \tilde{a}_{12} \nu^2, \quad (40)$$

with ²

$$\begin{aligned} p_0 &= 43.371638, & p_1 &= 929.579, \\ n_1 &= -1.174839, & p_2 &= -9178.87, \\ n_2 &= 0.354064, & p_3 &= 23632.3, \\ d_1 &= -0.151961, & p_4 &= -104.891. \end{aligned} \quad (41)$$

Similar to what will be seen to occur also for **SEOBNRv4**, the spin-dependence of the NR-informed parameters violates the clear distinction between spin-orbit and spin-spin Hamiltonians. In this case, c_3 introduces even-in-spin terms in $G_{S_*} \hat{S}_*$.

IV. THE HAMILTONIAN OF SEOBNRv4

The Hamiltonian used in the **SEOBNRv4** [8] model was structurally introduced in Ref. [19] for the case of generally oriented spins. In order to compare it to the **TEOBResumS** one, here we only focus on the spin-aligned case (the generic scenario is discussed in Appendix A).

The **SEOBNRv4** Hamiltonian is obtained as the result of a certain deformation of the Hamiltonian of a spinning particle on a Kerr background. First, the dimensionless BH spin \hat{a} is replaced by the effective spin \hat{S} (instead of $\tilde{a}_0 = \hat{S} + \hat{S}_*$ used in **TEOBResumS**). Second, the functions $(\Delta^K, \Sigma, \Lambda)$ entering the Kerr metric, Eq. (1), are deformed by adding ν -dependent PN information. These functions are resummed so as to obtain a robust behavior in the strong-field regime. Finally, one adds to the latter Hamiltonian additional terms that are obtained by similarly deforming the spin-orbit coupling function of a spinning particle on a Kerr BH.

We now denote the EOB Hamiltonian as

$$\hat{H}_{\text{EOB}} \equiv \frac{1}{\nu} \sqrt{1 + 2\nu \left(\hat{H}_{\text{eff}}^{\text{SEOB}} - 1 \right)}, \quad (42)$$

with $\hat{H}_{\text{eff}}^{\text{SEOB}}$ replacing the generic \hat{H}_{eff} of Eq. (21) and where, following Refs. [19, 21], we define the effective EOB Hamiltonian as

$$\hat{H}_{\text{eff}}^{\text{SEOB}} = \hat{H}_{\text{NS}} + \hat{H}_{\text{SO}} + \hat{H}_{\text{SS}}^{\text{eff}}. \quad (43)$$

Here, \hat{H}_{NS} denotes the (deformed) Hamiltonian of a non-spinning particle; \hat{H}_{SO} indicates the ν -deformed spin-orbit coupling of the spinning particle and $\hat{H}_{\text{SS}}^{\text{eff}}$ refers to an additional spin-spin contribution. In this respect one has to be aware that *part* of the spin-orbit and spin-spin interaction is also incorporated in \hat{H}_{NS} , as it is inherited by the structure of the Hamiltonian of a test-particle moving in a Kerr metric.

The aim of this section is to illustrate that it is possible to recast the spin-aligned Hamiltonian of **SEOBNRv4** in a way that is formally close to the one of **TEOBResumS** as defined in Eq. (22), modulo the additional spin-spin contribution. The final result will be an expression of the form

$$\hat{H}_{\text{eff}}^{\text{SEOB}} = \hat{\mathbb{H}}_{\text{orb}}^{\text{eff}} + \left(\bar{G}_S \hat{S} + \bar{G}_{S_*} \hat{S}_* \right) p_\varphi + \hat{H}_{\text{SS}}^{\text{eff}}, \quad (44)$$

where: (i) the orbital Hamiltonian $\hat{\mathbb{H}}_{\text{orb}}^{\text{eff}}$ is formally analogous to $\hat{H}_{\text{orb}}^{\text{eff}}$, although the metric functions and the centrifugal radius are replaced by different analytical expressions; (ii) similarly, the spin-orbit sector (i.e., odd-in-spins) will resemble the **TEOBResumS** one, with the gyrogravitomagnetic functions $(\bar{G}_S, \bar{G}_{S_*})$ replacing (G_S, G_{S_*}) being different both in the gauge choice and the resummation approach. By contrast, the even-in-spin terms, that in **TEOBResumS** are entirely contained in $\hat{H}_{\text{orb}}^{\text{eff}}$, are partly incorporated within $\hat{\mathbb{H}}_{\text{orb}}^{\text{eff}}$ and partly in $\hat{H}_{\text{SS}}^{\text{eff}}$, as detailed below.

² In the equal-mass case, since the last term is not symmetric under the exchange of χ_1 and χ_2 , c_3 is computed adopting the convention $|\chi_1| > |\chi_2|$.

A. Rewriting of \hat{H}_{NS} : the centrifugal radius \bar{r}_c

Following Ref. [19], \hat{H}_{NS} is written following the structure of Eq. (9) and reads

$$\hat{H}_{\text{NS}} = \alpha \sqrt{1 + \gamma^{ij} p_i p_j + Q_4(p) + \beta^i p_i}, \quad (45)$$

where $Q_4(p)$ is a PN term quartic in the momenta that will be defined below and vanishes in the Kerr limit. The functions $(\alpha, \beta_i, \gamma^{ij})$ have the same structure of Eqs. (6)–(8), but different explicit form, since the components of the ν -deformed metric introduced in Ref. [21], for equatorial orbits, are

$$g^{tt} = -\frac{\Lambda_t}{\Delta_t \Sigma}, \quad (46)$$

$$g^{rr} = \frac{\Delta_r}{\Sigma}, \quad (47)$$

$$g^{\theta\theta} = \frac{1}{\Sigma}, \quad (48)$$

$$g^{\varphi\varphi} = \frac{1}{\Lambda_t} \left(-\frac{\tilde{\omega}_{fd}^2}{\Delta_t \Sigma} + \Sigma \right), \quad (49)$$

$$g^{t\varphi} = -\frac{\tilde{\omega}_{fd}}{\Delta_t \Sigma}, \quad (50)$$

where

$$\Delta_t = r^2 \Delta_u, \quad (51)$$

$$\Delta_r = \Delta_t \mathbb{D}^{-1}, \quad (52)$$

$$\Lambda_t = (r^2 + \hat{S}^2)^2 - \hat{S}^2 \Delta_t, \quad (53)$$

$$\Sigma = r^2, \quad (54)$$

$$\tilde{\omega}_{fd} = 2 \hat{S} r, \quad (55)$$

which mimic the Kerr functions³ and the Kerr BH spin \hat{a} is replaced by the effective spin \hat{S} . Note that the function Δ^K appears in both the g^{tt} and the g^{rr} components of the Kerr metric. This implies that, in Kerr, Δ^K is also part of the B function. In EOB models the connection between the metric potentials is more complicated because of the presence of the D function. Hence, Δ^K was replaced by Δ_t in the g^{tt} metric component and by Δ_r that appears in g^{rr} . The ν -deformation is implemented as follows. At 4PN accuracy, we define the function

$$\Delta_t^{4\text{PN}} \equiv r^2 A_{\text{orb}}^{4\text{PN}}(u) + \hat{S}^2, \quad (57)$$

where the terms $1 - 2u$ appearing in the Kerr function Δ^K is replaced by the PN-expanded EOB orbital potential at 4PN accuracy, as obtained from Eq. (26) dropping the 5PN, effective, correction. In SEOBNRv4, the resummation procedure is implemented on the Δ_u function, that at 4PN reads

$$\Delta_u^{4\text{PN}} \equiv u^2 \Delta_t^{4\text{PN}} = A_{\text{orb}}^{4\text{PN}}(u) + u^2 \hat{S}^2. \quad (58)$$

³ In general, $\tilde{\omega}_{fd}$ reads

$$\tilde{\omega}_{fd} = 2 \hat{S} r + \nu \omega_{fd}^0 \hat{S} + \nu \omega_{fd}^1 \hat{S} r. \quad (56)$$

With respect to Eq. (36) of Ref. [21], we already gauge-fixed the two frame-dragging parameters to zero, i.e. $\omega_{fd}^0 = \omega_{fd}^1 = 0$.

Two Kerr-like horizons u_{\pm} are imposed and the residual function is then resummed using a global logarithmic function as

$$\Delta_u = \hat{S}^2 (u - u_+) (u - u_-) \times \left[1 + \nu \Delta_0 + \log \left(1 + \sum_{i=1}^5 \Delta_i u^i \right) \right]. \quad (59)$$

Here (Δ_0, Δ_i) are ν -dependent coefficients that are obtained imposing that the PN-expansion of Eq. (59) coincides with the one of Eq. (58), see Ref. [23]. The two horizons are placed at

$$r_{\pm} \equiv \frac{1}{u_{\pm}} = \left(1 \pm \sqrt{1 - \hat{S}^2} \right) (1 - K\nu), \quad (60)$$

where K is a free parameter in the model that is calibrated to NR simulations [8]. Note that also that the various functions (Δ_0, Δ_i) depend on this parameter and can be found in Appendix A of Ref. [17]. We also list them for completeness in our Appendix C.

Finally, the D function is also resummed using a global overall logarithm instead of the Padé approximant used in TEOBResumS. It reads

$$\mathbb{D} = [1 + \log(1 + 6\nu u^2 + 2(26 - 3\nu)\nu u^3)]^{-1}. \quad (61)$$

We can then rewrite Eq. (45) in the following form

$$\hat{H}_{\text{NS}} = \hat{\mathbb{H}}_{\text{orb}}^{\text{eff}} + \bar{G}_S^0 \hat{S} p_{\varphi}, \quad (62)$$

in which we defined the Kerr-like gyro-gravitomagnetic function \bar{G}_S^0 as

$$\bar{G}_S^0 \equiv \frac{\tilde{\omega}_{fd}}{\Lambda_t \hat{S}} = 2 u \bar{u}_c^2. \quad (63)$$

Moreover, the effective *orbital* Hamiltonian $\hat{\mathbb{H}}_{\text{orb}}^{\text{eff}}$ reads

$$\hat{\mathbb{H}}_{\text{orb}}^{\text{eff}} = \sqrt{\mathbb{A} \left(1 + p_{\varphi}^2 \bar{u}_c^2 + 2\nu(4 - 3\nu) u^2 \bar{p}_{r_*}^4 \right) + \bar{p}_{r_*}^2}, \quad (64)$$

where we expanded $Q_4(p) \equiv 2\nu(4 - 3\nu)u^2 \bar{p}_{r_*}^4$ and we now define the momentum conjugate to the tortoise radial coordinate as $\bar{p}_{r_*} \equiv \sqrt{\mathbb{A}/\mathbb{B}} p_r$. The functions $(\mathbb{A}, \mathbb{B}, \mathbb{Q})$ are expressed in terms of the ν -deformed metric functions as

$$\mathbb{A} \equiv \frac{\Delta_t \Sigma}{\Lambda_t} = \frac{\bar{u}_c^2}{u^2} \Delta_u, \quad (65)$$

$$\mathbb{B} \equiv \frac{\Sigma}{\Delta_r} = \frac{\mathbb{D}}{\Delta_u}, \quad (66)$$

$$\mathbb{Q} \equiv 1 + \gamma^{ij} p_i p_j = 1 + p_{\varphi}^2 \bar{u}_c^2 + \frac{\bar{p}_{r_*}^2}{\mathbb{A}}. \quad (67)$$

The functions $(\mathbb{A}, \mathbb{B}, \mathbb{D}, \mathbb{Q})$ are analogous to (A, B, D, Q) used within TEOBResumS and, although different, they reduce to the same corresponding Kerr functions in the $\nu \rightarrow 0$ limit. In Eq. (64) we also introduced $\bar{u}_c \equiv 1/\bar{r}_c$, where \bar{r}_c is a *new* centrifugal radius. This function is a ν -deformation of the Kerr r_c^K , but differs from the TEOBResumS one, r_c , and explicitly reads

$$\bar{r}_c^2 \equiv \frac{\Lambda_t}{\Sigma} = \frac{(r^2 + \hat{S}^2)^2}{r^2} - \hat{S}^2 \Delta_u. \quad (68)$$

Writing an *orbital* Hamiltonian for SEOBNrv4, $\hat{\mathbb{H}}_{\text{orb}}^{\text{eff}}$, that mimics $\hat{H}_{\text{orb}}^{\text{eff}}$ makes it clearer where the differences between the models arise, though the two expressions look formally the same. The functions (A, r_c) and (\mathbb{A}, \bar{r}_c) are different from one another, even if they correctly reproduce the corresponding Kerr functions when $\nu \rightarrow 0$. To understand how this is possible, let us go back to the definitions of the centrifugal radius r_c^K and of the potential A^K for the Kerr metric, Eqs. (10) and (11) respectively. These can be written in two, analytically equivalent, forms, namely

$$[r_c^K]^2 \equiv \frac{(r^2 + \hat{a}^2)^2}{r^2} - \hat{a}^2 \Delta^K \quad (69a)$$

$$= r^2 + \hat{a}^2 \left(1 + \frac{2}{r}\right), \quad (69b)$$

and

$$A^K \equiv \frac{(u_c^K)^2}{u^2} \Delta^K \quad (70a)$$

$$= (1 - 2u_c^K) \frac{1 + 2u_c^K}{1 + 2u}. \quad (70b)$$

In SEOBNrv4 one obtains \bar{r}_c and \mathbb{A} using Eqs. (69a) and (70a), without expanding the expression of Δ^K , and then substituting $\hat{a} \rightarrow \hat{S}$ and $\Delta^K \rightarrow \Delta_u$. On the other hand, in TEOBResumS r_c and A are obtained through Eqs. (69b) and (70b), where the expressions have been simplified and bear no memory of the original function Δ^K that appears in the Kerr metric. Then, one substitutes $\hat{a} \rightarrow \tilde{a}_0$ and $(1 - 2u_c^K) \rightarrow A_{\text{orb}}$. In conclusion, as well as different spin variable and resummation choices, \bar{r}_c differs from r_c because it contains additional ν -dependent corrections that come from Δ_u . Hence, although the two function share the same $\nu = 0$ limit, the spin-square contributions that they incorporate differ already at linear order in ν .

B. \hat{H}_{SO} and the spin-orbit sector

Let us turn now to rewriting \hat{H}_{SO} using a different notation consistent with the orbital part. Our starting point is \hat{H}_{SO} as given by Eq. (4.18) of Ref. [19] (and re-written in Appendix A). Once restricted to spin-aligned systems, this gives ⁴

$$\hat{H}_{\text{SO}} = \frac{e^{2\tilde{\nu} - \tilde{\mu}}}{\tilde{B}^2 \sqrt{\mathbb{Q}}} \left\{ e^{\tilde{\mu} + \tilde{\nu}} - \tilde{J} \tilde{B}' + \frac{1 + 2\sqrt{\mathbb{Q}}}{1 + \sqrt{\mathbb{Q}}} \tilde{J} \tilde{B} \tilde{\nu}' \right\} p_\varphi \hat{S}_*, \quad (71)$$

where the functions of Ref. [21] are connected to the metric ones as

$$e^{2\tilde{\mu}} = \Sigma = r^2, \quad e^{2\tilde{\nu}} = \frac{\Delta_t \Sigma}{\Lambda_t} = \mathbb{A}, \quad (72)$$

$$\tilde{B} = \sqrt{\Delta_t} = \sqrt{\mathbb{A}} \bar{r}_c, \quad \tilde{J} = \sqrt{\Delta_r} = \frac{r}{\sqrt{\mathbb{B}}}, \quad (73)$$

and the prime indicates derivative with respect to r . In addition, the ν -dependent PN results for the spin-orbit coupling functions are included in Eq. (71) through a (gauge-dependent) mapping [21] between the spin variables that naturally enter the PN-expanded effective Hamiltonian, (\hat{S}, \hat{S}_*) , that are used in TEOBResumS, and the effective spin variables $(\hat{\mathbb{S}}, \hat{\mathbb{S}}_*)$ that appear in SEOBNrv4. These spin quantities are intended to be the spin of an effective particle, $\hat{\mathbb{S}}_*$, moving around an effective Kerr BH whose spin is $\hat{\mathbb{S}}$. Following Ref. [21], such spin mapping is defined as

$$\hat{\mathbb{S}} = \hat{S} + \frac{1}{c^2} \Delta_\sigma^{(1)} + \frac{1}{c^4} \Delta_\sigma^{(2)}, \quad (74)$$

$$\hat{\mathbb{S}}_* = \hat{S}_* + \frac{1}{c^2} \Delta_{\sigma^*}^{(1)} + \frac{1}{c^4} \Delta_{\sigma^*}^{(2)} + \frac{1}{c^6} \Delta_{\sigma^*}^{(3)}, \quad (75)$$

where the functions $(\Delta_\sigma^{(i)}, \Delta_{\sigma^*}^{(i)})$ are gauge-dependent function that are chosen so to incorporate the high-order ν -dependent PN information. Ref. [21] fixes the gauge imposing that $\Delta_\sigma^{(1)} = \Delta_{\sigma^*}^{(2)} = 0$, so that

$$\hat{\mathbb{S}} \equiv \hat{S}. \quad (76)$$

On the other hand, the functions $\Delta_{\sigma^*}^{(1)}$ and $\Delta_{\sigma^*}^{(2)}$ are fixed in such a way that, once the SEOB Hamiltonian is PN-expanded, the spin-orbit PN contributions up to NNLO are correctly recovered. Moreover, the spin-orbit sector is NR-informed by an additional N³LO effective correction of the form

$$\Delta_{\sigma^*}^{(3)} = \frac{d_{\text{SO}} \nu}{r^3} \hat{S}, \quad (77)$$

whose explicit expression can be found below.

Using the definitions of Eqs. (72) and (73), \hat{H}_{SO} can be rewritten as

$$\hat{H}_{\text{SO}} = \mathbb{G}_{\mathbb{S}_*} p_\varphi \hat{\mathbb{S}}_*, \quad (78)$$

where we defined

$$\mathbb{G}_{\mathbb{S}_*} \equiv \frac{1}{(\bar{r}_c)^2} \left\{ \frac{\sqrt{\mathbb{A}}}{\sqrt{\mathbb{Q}}} \left[1 - \frac{(\bar{r}_c)'}{\sqrt{\mathbb{B}}} \right] + \frac{\bar{r}_c}{2(1 + \sqrt{\mathbb{Q}})} \frac{\mathbb{A}'}{\sqrt{\mathbb{A}\mathbb{B}}} \right\}, \quad (79)$$

that formally coincides with Eq. (15), having replaced the Kerr functions (A^K, B^K, Q^K, r_c^K) with $(\mathbb{A}, \mathbb{B}, \mathbb{Q}, \bar{r}_c)$.

We found it convenient to write the complete spin-orbit content of SEOBNrv4 in a form that is close to the one of TEOBResumS, so to similarly define two gyrogravitomagnetic functions. To do so, we define the complete spin-orbit sector of $\hat{H}_{\text{eff}}^{\text{SEOB}}$ as

$$\hat{\mathbb{H}}_{\text{SO}} = \left(\bar{G}_S^0 \hat{S} + \mathbb{G}_{\mathbb{S}_*} \hat{\mathbb{S}}_* \right) p_\varphi. \quad (80)$$

Since $\hat{\mathbb{S}}_*$ is a linear combination of (\hat{S}, \hat{S}_*) , one sees that the above function can be written precisely as the corresponding function in TEOBResumS, though the gyrogravitomagnetic functions will eventually be different. We see that the $\Delta_{\sigma^*}^{(i)}$ that appear in Eq. (75) are functions of (r, p_{r_*}, p_φ) , with some additional gauge-freedom that can be fixed at will (see below). These latter formally read

$$\Delta_{\sigma^*}^{(1)} = c_u u + c_Q (\mathbb{Q} - 1) + c_{p_r^2} \frac{p_r^2}{\mathbb{B}}, \quad (81)$$

$$\begin{aligned} \Delta_{\sigma^*}^{(2)} = & c_{u^2} u^2 + c_{Q^2} (\mathbb{Q} - 1)^2 + c_{u\mathbb{Q}} u (\mathbb{Q} - 1) + \\ & + c_{p_r^4} \frac{p_r^4}{\mathbb{B}^2} + c_{up_r^2} u \frac{p_r^2}{\mathbb{B}} + c_{p_r^2 \mathbb{Q}} \frac{p_r^2}{\mathbb{B}} (\mathbb{Q} - 1). \end{aligned} \quad (82)$$

⁴ Note that our notation differs from Ref. [21]. We define their ν as $\tilde{\nu}$, not to confuse it with the symmetric mass ratio. Also, we use explicitly $\tilde{B}_r = \tilde{B}' - \tilde{B}/\tilde{J}$ and $\mu_r = \mu' - 1/\tilde{J}$.

The explicit expression of the c_X coefficients can be obtained comparing Eqs. (81) and (82) to Eqs. (51) and (52) of Ref. [21] and are recalled in Appendix D. All these coefficients are linear functions of (\hat{S}, \hat{S}_*) . Thus, we can write $\Delta_{\sigma^*}^{(1)} = c_S^{(1)}\hat{S} + c_{S_*}^{(1)}\hat{S}_*$ and $\Delta_{\sigma^*}^{(2)} = c_S^{(2)}\hat{S} + c_{S_*}^{(2)}\hat{S}_*$, and, substituting them into Eq. (80), we obtain

$$\hat{\mathbb{H}}_{\text{SO}} \equiv (\bar{G}_S \hat{S} + \bar{G}_{S_*} \hat{S}_*) p_\varphi, \quad (83)$$

where we defined two *new* gyro-gravitomagnetic functions

$$\bar{G}_S \equiv \bar{G}_S^0 + (c_S^{(1)} + c_S^{(2)}) \mathbb{G}_{\mathbb{S}_*}, \quad (84)$$

$$\bar{G}_{S_*} \equiv (1 + c_{S_*}^{(1)} + c_{S_*}^{(2)}) \mathbb{G}_{\mathbb{S}_*}. \quad (85)$$

The explicit forms of $[c_S^{(i)}, c_{S_*}^{(i)}]$ are also reported in Appendix D. In inspecting those expressions, one should be aware that the two models adopt two different gauges in the spin-orbit sector. On the one hand, **TEOBResumS** is written in the DJS gauge [30, 34] that is designed to cancel all the dependence on p^2 in the gyro-gravitomagnetic functions. On the other hand, within **SEOBNRv4T** one makes the minimal gauge choice and sets all gauge parameters to be zero. More details can be found in Appendix E.

C. $\hat{H}_{\text{SS}}^{\text{eff}}$ and the spin-spin sector

Moving finally to the spin-spin sector, we define $\hat{H}_{\text{SS}}^{\text{eff}}$ as

$$\hat{H}_{\text{SS}}^{\text{eff}} = \hat{H}_{\text{SS}} - \frac{1}{2}u^3(\hat{S}_*)^2 + \frac{d_{\text{SS}}\nu}{r^4}(X_1^4\chi_1^2 + X_2^4\chi_2^2). \quad (86)$$

The first term in the r.h.s. of the above equation, for equatorial orbits (see Eq. (4.19) of Ref. [19] or Appendix A for generic ones) explicitly reads

$$\begin{aligned} \hat{H}_{\text{SS}} &= \omega \hat{S}_* + \frac{e^{-3\bar{\mu}-\bar{\nu}}\tilde{J}}{2\tilde{B}\sqrt{\mathbb{Q}}(1+\sqrt{\mathbb{Q}})} \times \\ &\times \left\{ e^{2\bar{\mu}+2\bar{\nu}}p_\varphi^2 + e^{2\bar{\mu}}\sqrt{\mathbb{Q}}(1+\sqrt{\mathbb{Q}})\tilde{B}^2 - \tilde{J}^2p_r^2\tilde{B}^2 \right\} \omega' \hat{S}_*, \end{aligned} \quad (87)$$

where

$$\omega \equiv \frac{\tilde{\omega}_{fd}}{\Lambda_t} = \bar{G}_S^0 \hat{S}. \quad (88)$$

Using Eqs. (72), (73) and (88), \hat{H}_{SS} can be rewritten as

$$\begin{aligned} \hat{H}_{\text{SS}} &= \left\{ \bar{G}_S^0 + \frac{\bar{r}_c}{2\sqrt{\mathbb{B}}} \left[1 - \frac{1}{\sqrt{\mathbb{Q}}(1+\sqrt{\mathbb{Q}})} \times \right. \right. \\ &\times \left. \left. \left(p_\varphi^2 \bar{u}_c^2 - \frac{p_{r_*}^2}{\mathbb{A}} \right) \right] (\bar{G}_S^0)' \right\} \hat{S} \hat{S}_*. \end{aligned} \quad (89)$$

The second term in the r.h.s. of Eq. (86) was introduced in Ref. [19] [see Eqs. (5.59), (5.60) and (5.70) therein and related discussion] to correctly account for the LO spin-spin coupling. One easily checks that PN-expanding the whole $\hat{H}_{\text{SS}}^{\text{eff}}$ together with $\hat{\mathbb{H}}_{\text{orb}}^{\text{eff}}$ is necessary to correctly

recover the LO spin-spin contribution in the full Hamiltonian, $\hat{H}_{\text{SS}}^{\text{LO}} = -u^3(\hat{S} + \hat{S}_*)^2/2 = -\tilde{a}_0^2/2$. This constitutes the main structural difference between **TEOBResumS** and **SEOBNRv4** in the spin-spin sector. In fact, in the former even-in-spin terms are fully resummed through r_c , while in the latter these terms are partially resummed within \bar{r}_c and partly added to the Hamiltonian as they are.

We also note in passing that, by expanding $\mathbb{H}_{\text{orb}}^{\text{eff}}$, one also finds the Kerr-like quartic-in-spin term $\hat{S}^4/2$. This term takes into account only a fraction of the analytically known LO quartic-in-spin Hamiltonian. By contrast, it was shown in Ref. [11] that this is completely incorporated in the **TEOBResumS** Hamiltonian because of the use of effective spin \tilde{a}_0 within r_c .

Finally, Eq. (86) also features the presence of an effective NLO spin-spin correction, with the adjustable parameter d_{SS} that will be discussed below.

D. Numerical relativity calibrated functions

As briefly mentioned above, the **SEOBNRv4** analytic structure is completed by 3 functions that are calibrated to NR simulations. These functions are: (i) K , that enters Δ_u ; (ii) d_{SO} , that is found in the definition of the effective spin variable \hat{S}_* ; and (iii) d_{SS} that affects the spin-spin coupling. The NR-calibrated expression of K was obtained in Ref. [8] and reads

$$K = K|_{\chi=0} + K|_{\chi \neq 0}, \quad (90)$$

where we introduced the functions

$$\begin{aligned} K|_{\chi=0} &= 267.788247\nu^3 - 126.686734\nu^2 + 10.257281\nu + \\ &+ 1.733598, \end{aligned} \quad (91)$$

$$\begin{aligned} K|_{\chi \neq 0} &= -59.165806\chi^3\nu^3 - 0.426958\chi^3\nu + 1.436589\chi^3 + \\ &+ 31.17459\chi^2\nu^3 + 6.164663\chi^2\nu^2 - 1.380863\chi^2 + \\ &- 27.520106\chi\nu^3 + 17.373601\chi\nu^2 + 2.268313\chi\nu + \\ &- 1.62045\chi, \end{aligned} \quad (92)$$

where

$$\chi \equiv \chi_S + X_{12} \frac{\chi_A}{1-2\nu} = \frac{\hat{S}}{X_1^2 + X_2^2}, \quad (93)$$

with $\chi_S = (\chi_1 + \chi_2)/2$ and $\chi_A = (\chi_1 - \chi_2)/2$. The spin-orbit sector presents an additional N³LO effective correction that reads

$$\begin{aligned} d_{\text{SO}} &= 147.481449\chi^3\nu^2 - 568.651115\chi^3\nu \\ &+ 66.198703\chi^3 - 343.313058\chi^2\nu \\ &+ 2495.293427\chi\nu^2 - 44.532373. \end{aligned} \quad (94)$$

Finally, the NLO effective spin-spin correction that enters $\hat{H}_{\text{SS}}^{\text{eff}}$ is NR-calibrated through the parameter

$$\begin{aligned} d_{\text{SS}} &= 528.511252\chi^3\nu^2 - 41.000256\chi^3\nu \\ &+ 1161.780126\chi^2\nu^3 - 326.324859\chi^2\nu^2 \\ &+ 37.196389\chi\nu + 706.958312\nu^3 \\ &- 36.027203\nu + 6.068071. \end{aligned} \quad (95)$$

As all these coefficients depend on multiple powers of the individual spins, a clear distinction between the spin-orbit and spin-spin sectors is impossible.

V. SELECT COMPARISON BETWEEN TEOBRESUMS AND SEOBNRV4

We have seen that the TEOBResumS and SEOBNrv4 Hamiltonians are constructed rather differently. They differ in the amount of analytical information that is included, the spin-gauge, the resummation procedures and the way they are informed (or calibrated) to NR simulations. Still, both models deliver waveforms that are *faithful* with state-of-the-art NR simulations at 1% level or better [8, 10]. This is possible because, on top of the tunable functions that enter the dynamics of the two models, (a_6^c, c_3) and $(K, d_{\text{SO}}, d_{\text{SS}})$ the waveforms are also NR-completed through merger and ringdown in some way. The aim of this section is to attempt to quantify the differences entailed by the two NR-informed Hamiltonians. To do so, we focus on the gauge-invariant relation between energy and angular momentum (or orbital frequency) and we calculate them both in the adiabatic approximation as well as non-adiabatically, switching on some analytical radiation reaction to account for the angular momentum losses.

A. Adiabatic dynamics

Our interest is to make some comparative statements between the dynamics of the two models. Since the models are calibrated to NR, and moreover are expressed in different gauges, direct comparisons between the analytical expressions discussed above are not informative. On the contrary, comparisons between gauge-invariant quantities are meaningful and we start by considering the *adiabatic* approximation to the dynamics, i.e. a sequence of circular orbits. We hence set $p_{r_*} = 0$ and compute, at each given radius, the circular angular momentum p_φ^{circ} solving $\partial \hat{H}_{\text{eff}}(r, p_\varphi^{\text{circ}})/\partial r = 0$. We can then compare the rescaled binding energy of a system $\hat{E}_b \equiv (E - M)/\mu$ of the two models, when plotted as a function of the angular momentum p_φ or of the dimensionless orbital frequency $\Omega \equiv M\Omega_{\text{phys}} = \partial \hat{H}_{\text{EOB}}/\partial p_\varphi$.

The results of these comparisons are shown in Fig. 1. From simplicity, in the following we will often denote TEOBResumS as TEOB and SEOBNrv4 as SEOB. The markers highlight the location of the last stable orbit (LSO), which corresponds to the inflection point of the Hamiltonian and is thus found imposing $\partial \hat{H}_{\text{eff}}/\partial r = \partial^2 \hat{H}_{\text{eff}}/\partial r^2 = 0$. As expected, the binding energies are similar but not exactly overlapping. It is difficult to quantify the effects of this difference, but it is probably tapered in the full models, when taking into account the respective radiation reactions. In the next section, we will compare binding energy in the non-adiabatic scenario, adding the same radiation reaction to both models.

The general characteristics of the dynamics can be also summarized by inspecting various gauge-invariant quantities at the LSO, i.e. binding energy, orbital frequency and the dimensionless Kerr parameter

$$\chi_J \equiv \frac{1}{\nu} \frac{j_{\text{tot}}}{\hat{H}_{\text{EOB}}^2}, \quad (96)$$

where j_{tot} is total angular momentum and reads

$$j_{\text{tot}} = p_\varphi + \frac{X_1}{X_2} \chi_1 + \frac{X_2}{X_1} \chi_2. \quad (97)$$

This is done in Fig. 2, that refers to the equal-mass, equal-spin case. On the x -axis we put $\tilde{a}_0 = \chi_1 = \chi_2$. Note that the curve for TEOBResumS stops at $\tilde{a} \approx 0.7$ because the LSO does not exist for higher spins. We will comment more on this aspect in the conclusions. It is interesting to note that for large, positive spins TEOBResumS predicts values of the LSO frequency larger than the SEOBNrv4 ones.

The last piece of information that can be extracted from the two Hamiltonians in the adiabatic case concerns the spin-orbit and spin-spin contributions. In fact, if we consider small spins, $\tilde{a}_i \ll 1$, we can expand the Hamiltonian as

$$\begin{aligned} \hat{H}_{\text{EOB}}(\nu, \tilde{a}_1, \tilde{a}_2) &\sim E_0(\nu) + E_{\tilde{a}_1}(\nu) \tilde{a}_1 + E_{\tilde{a}_2}(\nu) \tilde{a}_2 + \\ &+ E_{\tilde{a}_1^2}(\nu) \tilde{a}_1^2 + E_{\tilde{a}_1 \tilde{a}_2}(\nu) \tilde{a}_1 \tilde{a}_2 + \\ &+ E_{\tilde{a}_2^2}(\nu) \tilde{a}_2^2 + \mathcal{O}[\tilde{a}_i^3]. \end{aligned} \quad (98)$$

In this situation, the E_X functions are well defined and depend on the mass ratio and dynamical variables but not on the spin values. These functions hence encode the way the linear and quadratic-in-spin terms are described in the two models. We can obtain each contribution analytically differentiating \hat{H}_{EOB} , e.g. $E_{\tilde{a}_1} = (\partial \hat{H}_{\text{EOB}}/\partial \tilde{a}_1)|_{\tilde{a}_i=0}$. For simplicity, we instead compute them numerically, considering very small (positive or negative) spins and suitably summing/subtracting the corresponding energies so to obtain the coefficients. For example, $E_{\tilde{a}_1} = [\hat{H}_{\text{EOB}}|_{(\tilde{a}_1=a, \tilde{a}_2=0)} - \hat{H}_{\text{EOB}}|_{(\tilde{a}_1=-a, \tilde{a}_2=0)}]/(2a)$, with $a \sim 10^{-4}$.

Note that in the adiabatic case, using p_φ as a variable is problematic, as it presents a cusp at the LSO, when the stable and unstable orbits branches meet. Moreover, the spin-squared contributions are singular at the same point when plotted versus the angular momentum. Conversely, the orbital frequency is continuous and well-behaved near the LSO, making it more useful for comparisons. The results for equal-mass systems are exhibited in Fig. 3.

The figure illustrates that $E_{\tilde{a}_1}$ is reasonably consistent between the two models, although it has a slightly different behavior after the nonspinning LSO. $E_{\tilde{a}_1^2}$, instead, is completely different. The two curves behave similarly in the PN regime (for small values of Ω) but quickly start to disagree and even change sign well before the LSO. Some difference was to be expected due to the different included PN information and way to include spin-spin terms within the EOB framework.

Since these functions are universal, we can extract the linear-in-spin contribution for any value of the spins as $E_{\tilde{a}_1} \tilde{a}_1 + E_{\tilde{a}_2} \tilde{a}_2$, even if for large spins the expansion of Eq. (98) is no longer valid and higher order contributions become non-negligible. Thus, we expect that these differences will be more pronounced for large aligned spins, when the LSO occurs at higher frequencies.

As a consistency test, we show in Fig. 4 the same comparison for $q = 5$, together with the Kerr corresponding curves. As expected, since the two models share the same $\nu \rightarrow 0$ and PN limits, in this case the curves have a similar behavior and are close to the Kerr functions.

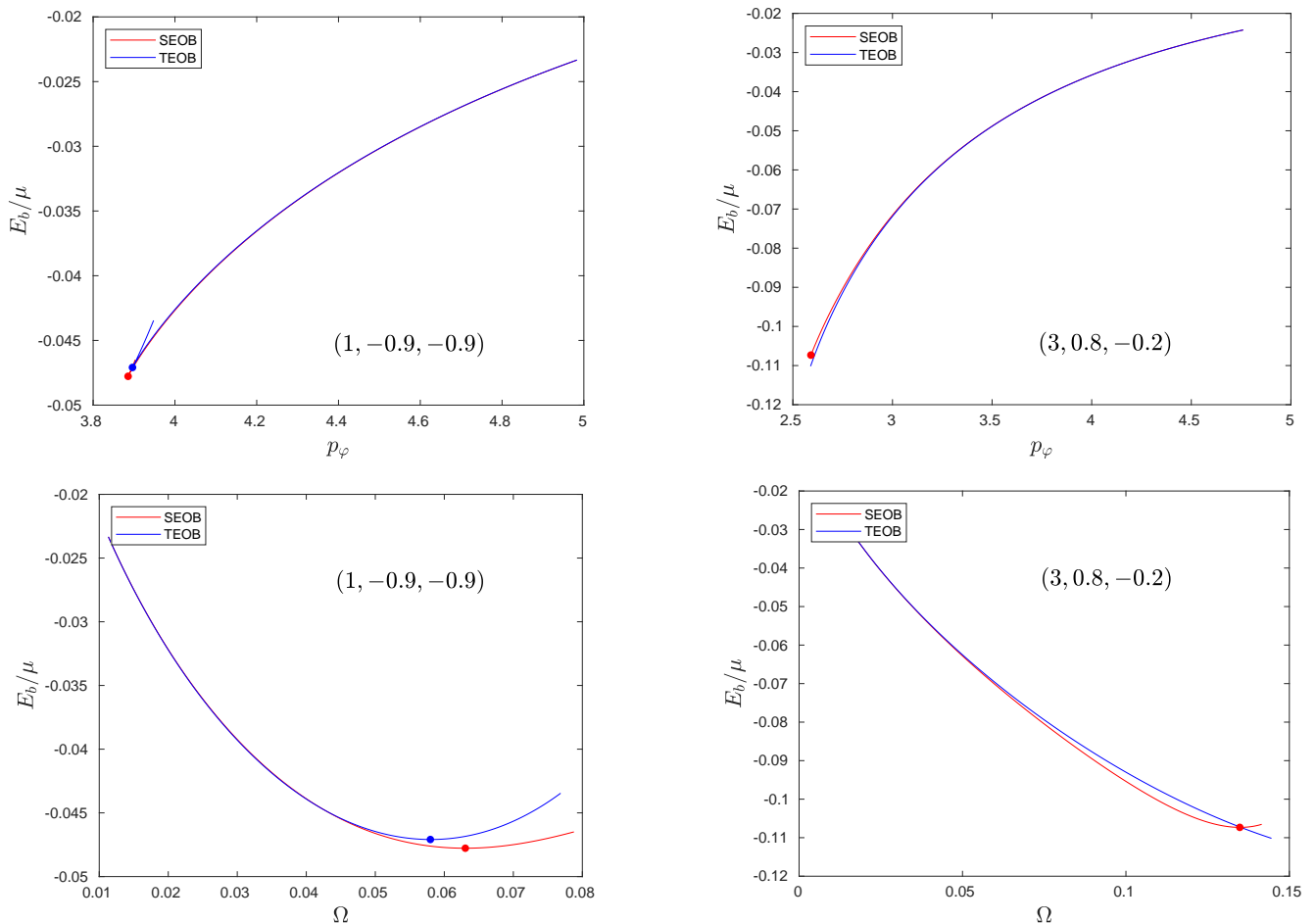


FIG. 1. Gauge-invariant relation between E_b and p_φ and Ω in the adiabatic case. The markers correspond to the LSO position (not present in **TEOBResumS** for large aligned spins).

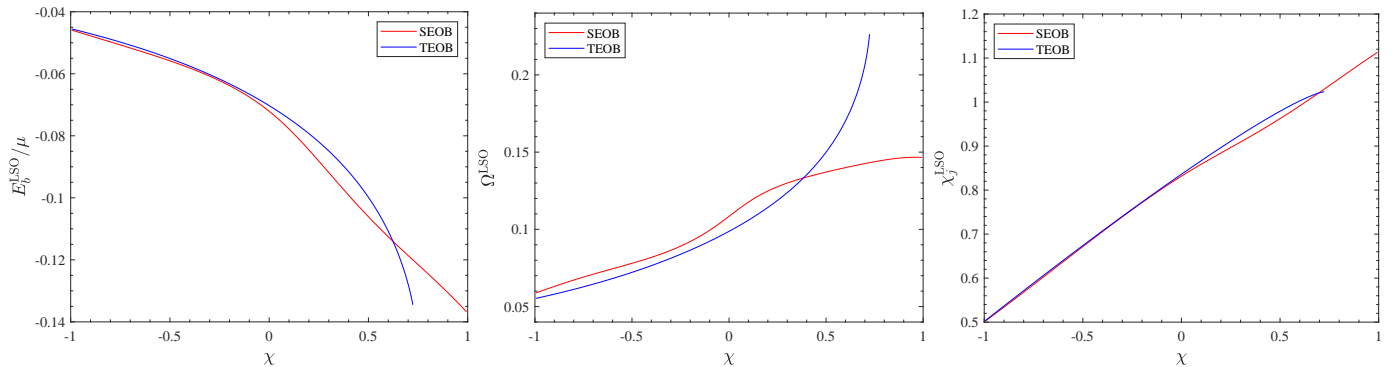


FIG. 2. Gauge-invariant quantities computed at the LSO for $q = 1$. Note that the **TEOBResumS** Hamiltonian does not have an LSO after $\chi \approx 0.7$ and thus the corresponding curves terminate there.

As we briefly mentioned in the previous sections, the NR-informed parameters introduce a complicated spin-dependence in both models. In order to remove these effects, we compare in Fig. 5 the LSO quantities for **TEOBResumS** and **SEOBNRv4**, after eliminating the NR-calibration, i.e. we impose $a_6^c = c_3 = 0$ and $K = d_{SS} = d_{SO} = 0$ respectively. Two features become evident: (i) **TEOBResumS** does not display an LSO for $\chi \geq 0.3$; (ii) **SEOBNRv4** has a behavior that is Kerr-like and does not display a change of concavity.

We conclude this section by showing in Fig. 6 the com-

parisons between $E_{\bar{a}_1}$ and $E_{\bar{a}_2}$. We can see that the main effect of using NR information is a decrease in the importance of the spin terms. However, NR-calibrated terms also change the behavior of the spin interaction. Without these, the **TEOBResumS** and **SEOBNRv4** curves are closer and $E_{\bar{a}_1}$ is positive for both models up to the LSO.

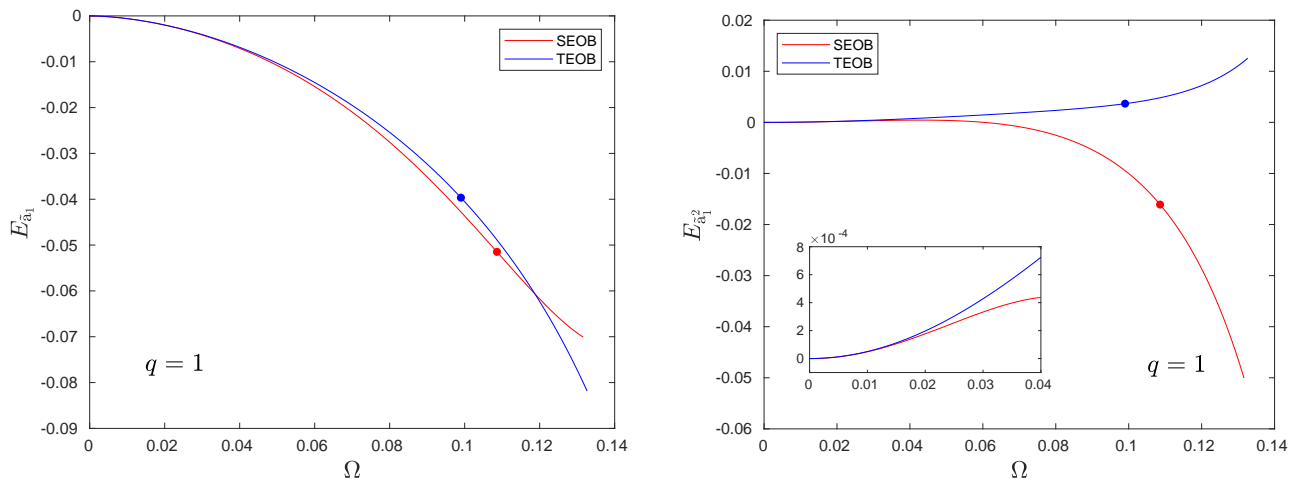


FIG. 3. Linear and quadratic-in-spin Hamiltonian contributions in the equal-mass case. $E_{\bar{a}_1}$ qualitatively agrees between the two models. The quadratic-in-spin behaviour is instead completely different, although it is similar in the PN regime. We remind the reader that for these systems $E_{\bar{a}_1} = E_{\bar{a}_2}$ and $E_{\bar{a}_1^2} = E_{\bar{a}_2^2}$, while $E_{\bar{a}_1\bar{a}_2}$, though not shown, displays a similar behavior to $E_{\bar{a}_1^2}$. The markers highlight the nonspinning LSO position.

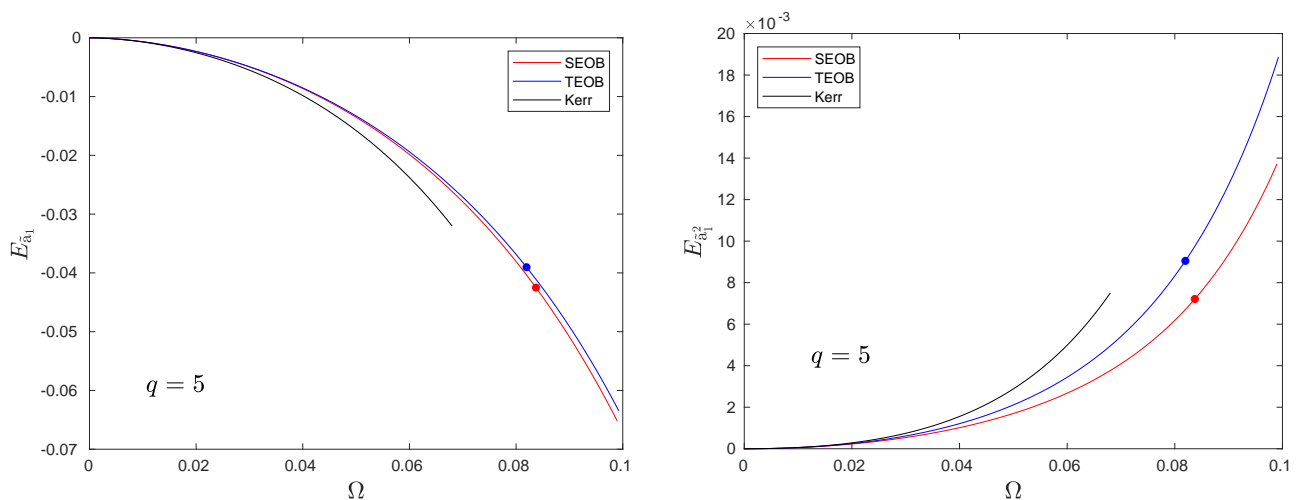


FIG. 4. Same as Fig. 3 for systems of $q = 5$. We also added the Kerr corresponding functions up to the Schwarzschild LSO. In this case, all three curves agree qualitatively.

B. Non adiabatic dynamics

Let us now complement the above section with similar comparisons based on *non-adiabatic* evolutions, so to get up to merger. To do so, for both Hamiltonians we write Hamilton's equations with the *same* radiation reaction \mathcal{F}_φ . For consistency between TEOBResumS and SEOBNRv4T, we use the formal expression of \mathcal{F}_φ discussed in Ref. [10], where however the argument x is taken to be $x = \Omega^2(\Omega|_{p_r=0})^{-4/3}$. We stress that this choice does not correspond to neither the TEOBResumS nor the SEOBNRv4 one. The purpose of this section is to purely explore the structure of the Hamiltonians in the strong field, and compare them. It is intended that the full energetics obtained from this dynamics is not expected to be fully compatible with the corresponding NR one, like it is for the NR-completed model [26]. Similarly, we don't improve the inspiral EOB analytical waveform with a NR-improved description of the merger (i.e., next-to-quasi-circular cor-

rections) nor ringdown, but we adopt it as is. However, since its amplitude has a peak that is known to be close (both in location and amplitude) to the actual merger point obtained by NR simulations, we use it as an *approximate* merger point (note that this is the choice usually adopted in the analytical description of coalescing and merging BNS). Such approximate merger location will be useful below. Fig. 7 compares the relation $E_b(p_\varphi)$ of the two models for a few configurations. The approximate merger point (as defined above) for each model is shown as a colored marker. One sees that, on randomly chosen configurations, the global differences are non negligible. In particular, they are larger than the expected uncertainty on the corresponding NR curves ($\sim 10^{-4}$). Moreover, the position of the (2, 2) peak is often very different, with TEOBResumS merging later for large aligned spins and sooner for anti-aligned ones.

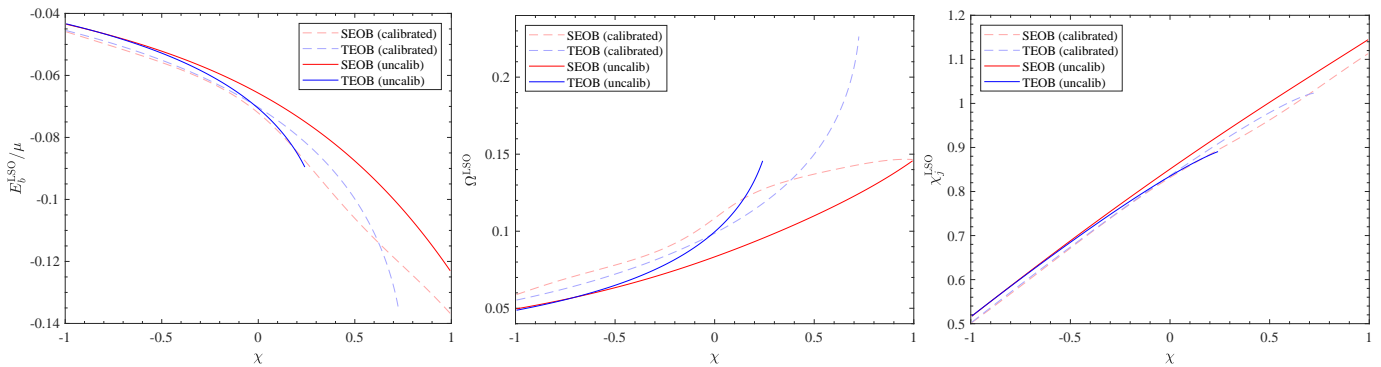


FIG. 5. Same as Fig. 2 using models without NR information, i.e. setting all calibration coefficients to zero. The NR-informed **TEOBResumS** and **SEOBNRv4** are indicated with dashed lines. Without calibration, **TEOBResumS** does not have an LSO after $\chi \approx 0.3$.

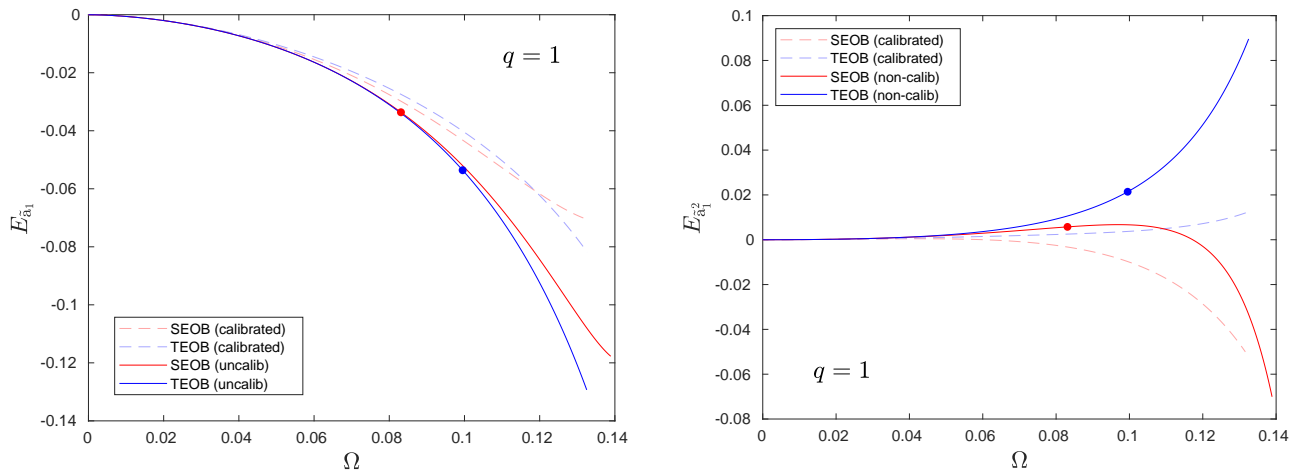


FIG. 6. Comparison of $E_{\bar{a}_1}$ and $E_{\bar{a}_1}^2$ for **TEOBResumS** and **SEOBNRv4** without NR calibration. The dashed lines correspond to the curves of Fig. 3. It is possible to notice how the non-calibrated curves are closer and have a more similar behavior up the LSO. Moreover, we can see that both the spin-orbit and spin-spin interactions are tempered by the use of NR information.

C. Modifying the resummation of the A -potential of **TEOBResumS**: EOB/NR phasing and unfaithfulness

We have seen above that, due to the several structural differences between the two models, it is difficult to understand clearly what special physical element is responsible for some specific dynamical behavior. Generally speaking one sees that the two models implement a fundamentally different description of the spin-spin interaction and this eventually reflects on all diagnostics that we have analyzed.

To shed more light on the impact of the various analytical structure, we focus here on a specific analytical element, the A potential, and explore the consequences of its resummation. We do so considering only the *nonspinning* sector of **TEOBResumS** and **SEOBNRv4** by performing the following exercise: we replace the Padé resummed A potential of **TEOBResumS** by the log-resummed one of **SEOBNRv4**, with some undetermined value of the parameter K . We ask then the following question: is it possible to tune the value of K within such potential to obtain a new, NR-faithful, nonspinning EOB model *without* changing anything else? As a reference waveform model with a Padé resummed potential we use here the improved nonspinning version of **TEOBResumS**, called of **TEOBiResumMultipoles**,

introduced in Ref. [35]. Analytically, the model features an improved description of the multipolar waveform amplitude (and thus radiation reaction) that in general incorporate up to 6PN test-mass information in Padé resummed form. The only change we adopt here with respect to that model is that the residual waveform amplitude ρ_{22}^{orb} is kept in its Taylor-expanded form at 3^{+2} PN accuracy. In addition, the model is based on an improved determination of a_6^c , partly due to the different analytical framework and partly due to the comparison with NR simulations with smaller numerical uncertainties. Moreover, **TEOBiResumMultipoles** also incorporates all modes up to $\ell = m = 5$ (included) completed through merger and ringdown. To determine the new values of K we follow the procedure discussed in Ref. [35]: we align the EOB and NR waveforms in the early inspiral and then determine K so that the EOB/NR phase difference at merger is of the order of the numerical uncertainty. In doing so, we also keep attention that the corresponding behavior of the EOB frequencies during the plunge is consistent with the NR one. We do so on seven mass ratios $q = \{1, 2, 2.5, 3, 6, 8, 18\}$ and determine some good values of K . These values are then fitted with the following func-

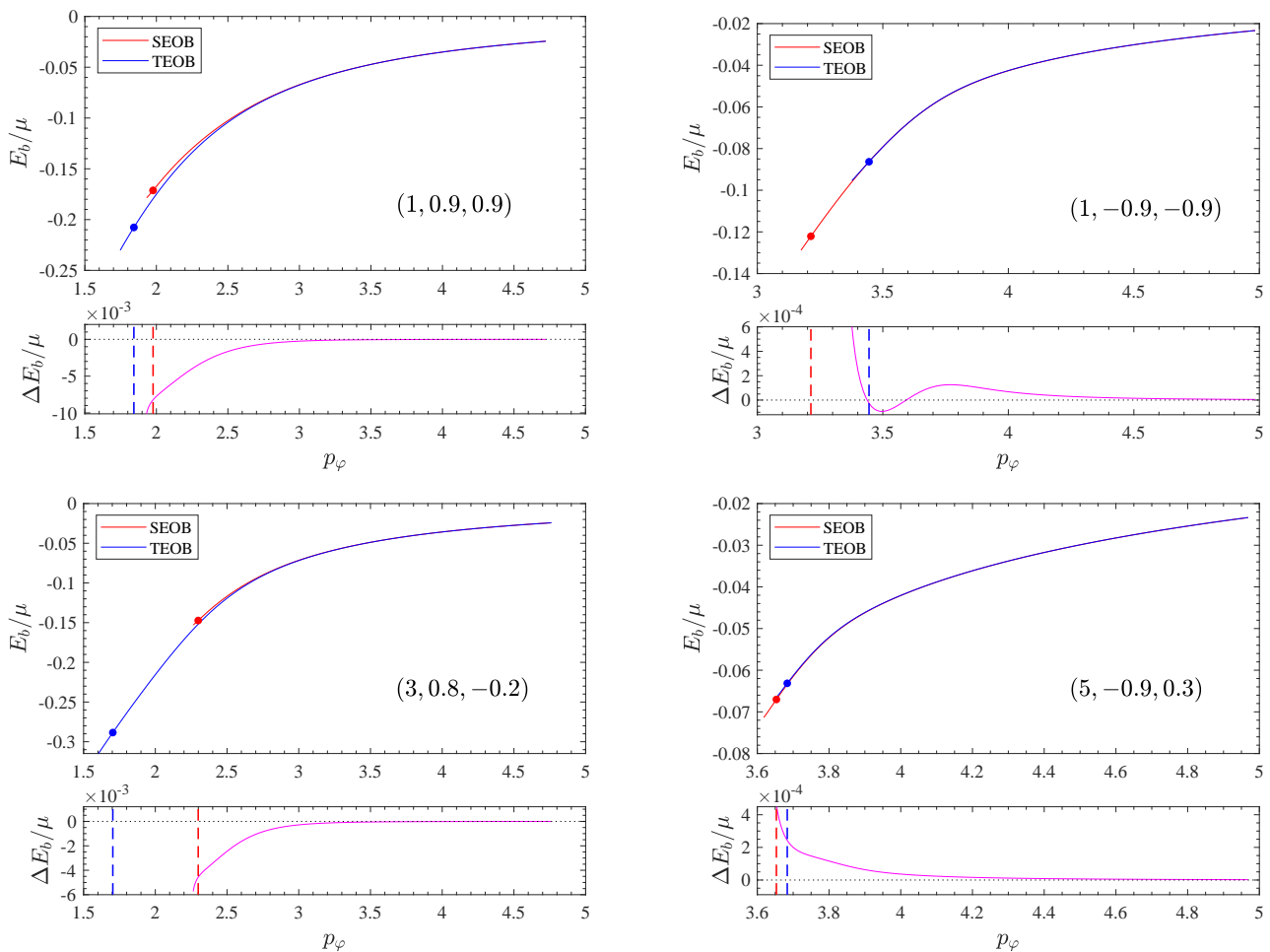


FIG. 7. Non-adiabatic evolution: gauge-invariant relation between binding energy E_b/μ and orbital angular momentum p_ϕ obtained using the two different **TEOBResumS** and **SEOBNRv4** Hamiltonians, but the same radiation reaction. The markers highlight the position of the peak of the (2, 2) mode. The lower panel shows the difference $\Delta E_b/\mu = (E_b^{\text{TEOB}} - E_b^{\text{SEOB}})/\mu$.

tional form

$$K = k_0 \frac{1 + n_1\nu + n_2\nu^2}{1 + d_1\nu + d_2\nu^2} \quad (99)$$

where the fitted parameters are

$$\begin{aligned} k_0 &= 0.13707, \\ n_1 &= 191.5614, \\ n_2 &= -221.8992, \\ d_1 &= -12.2328, \\ d_2 &= 187.6895. \end{aligned} \quad (100)$$

Just as a illustrative comparison, the left panel of Figs. 8 and 9 exhibit the EOB/NR $\ell = m = 2$ phasing comparison obtained with **TEOBiResumMultipoles** and with its *K*-avatar. The right panels of the same figures also show the corresponding $\ell = m = 2$ and $\ell = 2, m = 1$ amplitude and frequency. Following the approach of Ref. [35], to which we refer the reader for additional details, we show together the (i) bare EOB waveform (orange, dashed); (ii) the NQC completed one (blue, dash-dotted) and (iii) the complete waveform with the postmerger (postpeak) part (red-dashed). The most interesting result concerns the (2, 1) mode. The figure pinpoints the fact that, while for TEOB the NQC basis is efficient in correcting the ω_{21} frequency

so to allow a smooth connection to the ringdown part, it is unable to do so also when the log-resummed *A* potential is used. The reason for this behavior can be traced back on the structure of the NQC basis, that depends on the inverse of the orbital frequency. For the Padé-resummed *A* function, Ω decreases in a relatively mild way after its peak; on the contrary, for the log-resummed potential the decrease of Ω is very sharp, until it crosses zero very close to the (2, 1) waveform peak. At a practical level, the fact that $\Omega \simeq 0$ when the relative separation r is small, though finite, implies that the frequency-related NQC functions $n_3^{21} \equiv p_{r_*}/(r\Omega)$ and $n_4^{21} \equiv p_{r_*}/(r\Omega)\Omega^{2/3}$ (see [35]) become very large and prevent the related NQC correction to the phase to act efficiently so to correctly modify the circular EOB waveform.

To have an idea of the reliability of our new *K*-resummed EOB model, we computed EOB/NR faithfulness curves versus total mass, and also compared it with the **TEOBiResumSMultipoles**, see Fig. 10. We follow precisely the procedure and notation of Ref. [35], to which we refer the reader for details. It is interesting to note that \bar{F} has worsened with respect to the Padé resummed case, although it is still well below the usually accepted threshold of 1%. Also, one should note that the global shape of the curves is different, with the **TEOBResumS** ones

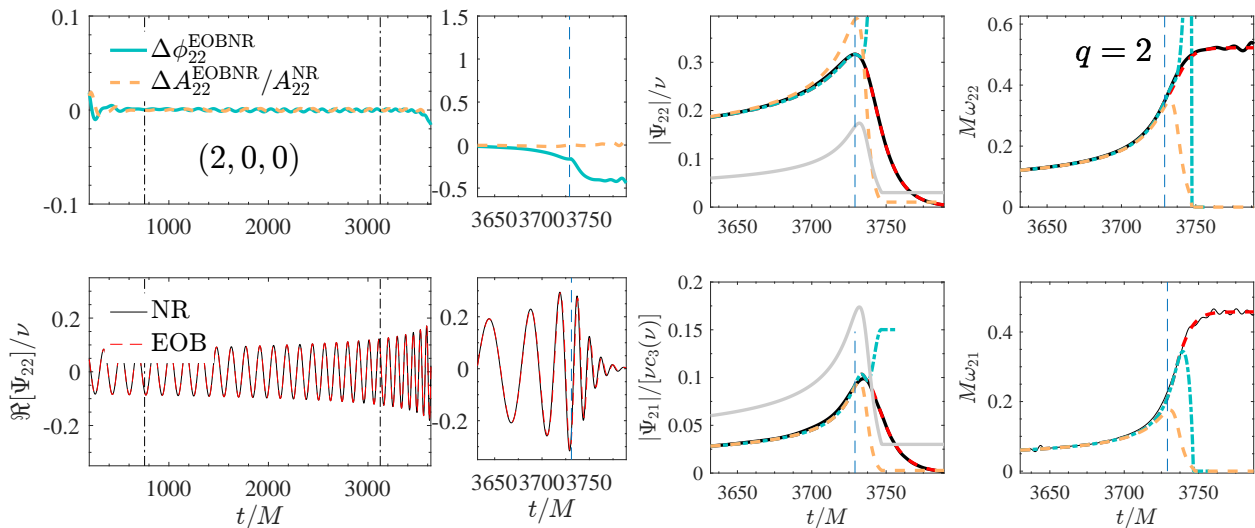


FIG. 8. EOB/NR phasing comparison with `TEOBiResumMultipoles` [35], with the Padé resummed A potential. Left panel: the $(2,2)$ phasing. Right panel, $(2,2)$ and $(2,1)$ amplitude and frequency. The plots also show: (i) the orbital frequency (gray lines); (ii) the bare EOB inspiral waveform (orange); (iii) the NQC improved waveform (blue); (iv) the NQC-ringdown completed waveform (red). The EOB/NR consistency for the $(2,1)$ mode is excellent.

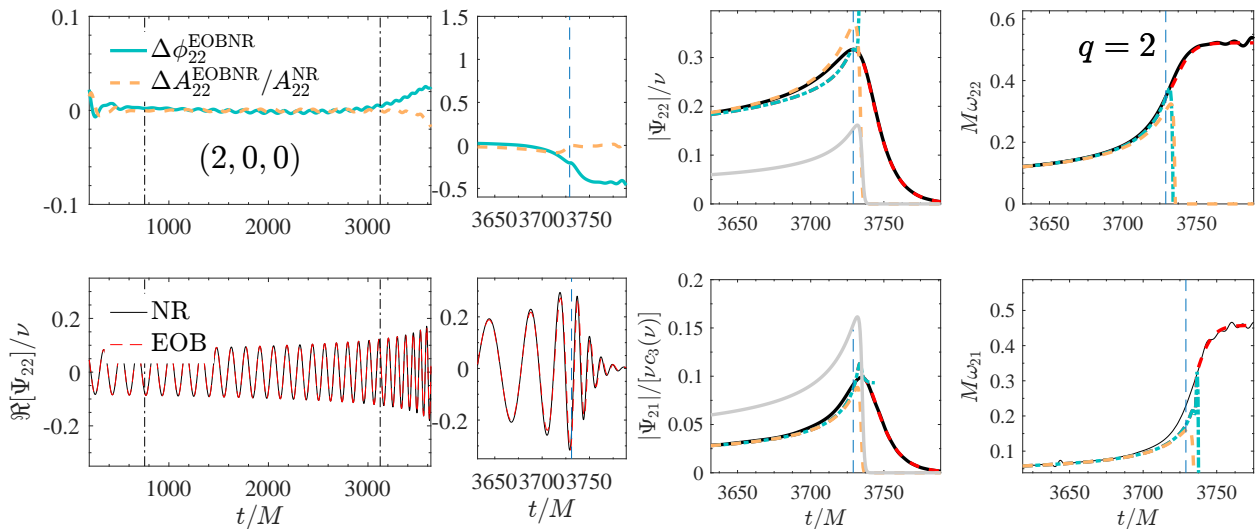


FIG. 9. Same as Fig 8 where the Padé resummed potential was replaced by the log-resummed potential with K given by Eq. (99). Though the agreement between the $(2,2)$ mode is rather acceptable, the NQC correction to the EOB instantaneous frequency is unable to provide a smooth matching with the postpeak part. This feature is related to the drop of the orbital frequency (gray line), that is much faster than the `TEOBResumS` one in Fig. 8; such behavior stems from the shape of the log-resummed A potential. See text for additional discussion.

being essentially monotonic. This illustrates the worsening of the model (or sometimes also of the NR waveform) during the ringdown, to which one is sensitive for large values of the masses. Such clear trend is not evident for the log-resummed potential (except for the $q = 18$ case): the curve have a maximum and it is not possible an immediate, intuitive, explanation of what is seen.

VI. POST ADIABATIC DYNAMICS

Despite being semi-analytical, EOB models improved by NR information are, generally, too slow to perform a parameter estimation run in a reasonable time. In order to

speed them up, reduced-order modeling [8, 36–40] versions of both `SEOBnrV4T` [8] and `TEOBResumS` [40] were built.

An alternative route to improve the computational efficiency of long-inspiral waveforms was proposed in Ref. [28], taking advantage of the post-adiabatic (PA) approximation to obtain the inspiral dynamics. The most expensive part of an EOB-waveform evaluation is in fact represented by the solution of the ODE system of the four Hamilton’s equation, that are solved with standard Runge-Kutta routines. The PA approximation can be used to analytically (though approximately) solve two of the four Hamilton’s equations on a sparse radial grid and obtain the system momenta. Two quadratures allow then one to obtain the time, the orbital phase and thus the

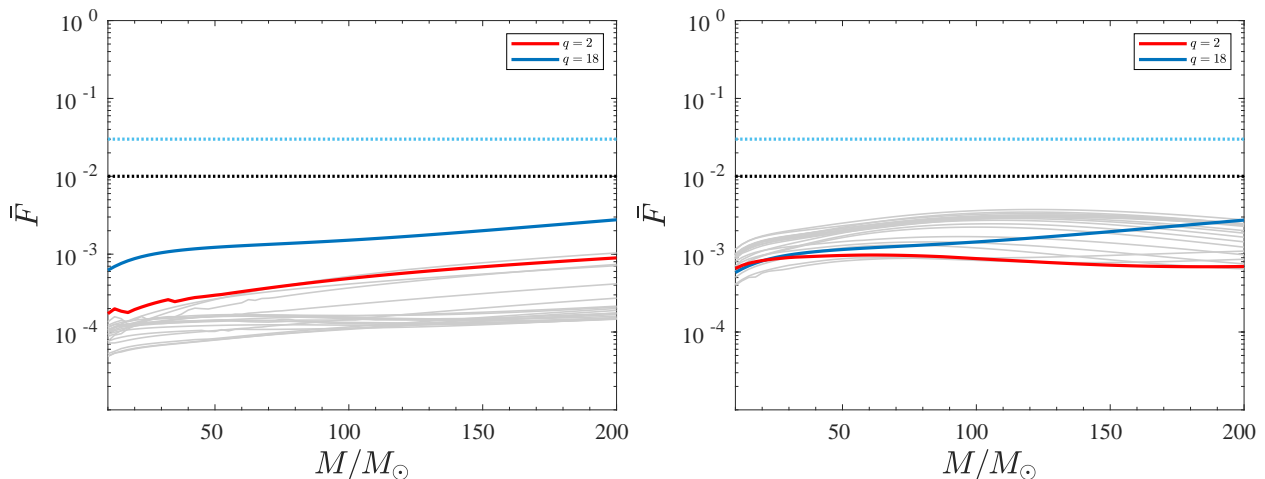


FIG. 10. EOB/NR unfaithfulness \bar{F} computation for the (2,2) mode with the Padé resummed potential (left panel) and the log-resummed potential (right-panel). We are collecting here all SXS NR simulations considered in Ref. [35], that span the mass ratio range $1 \leq q \leq 10$, plus a BAM dataset with $q = 18$. Although $\max(\bar{F})$ is well below the 1% threshold, the behavior of the function \bar{F} between the two potentials is actually very different. The red lines highlight the $q = 2$ data of Figs. 8-9. See text for discussion.

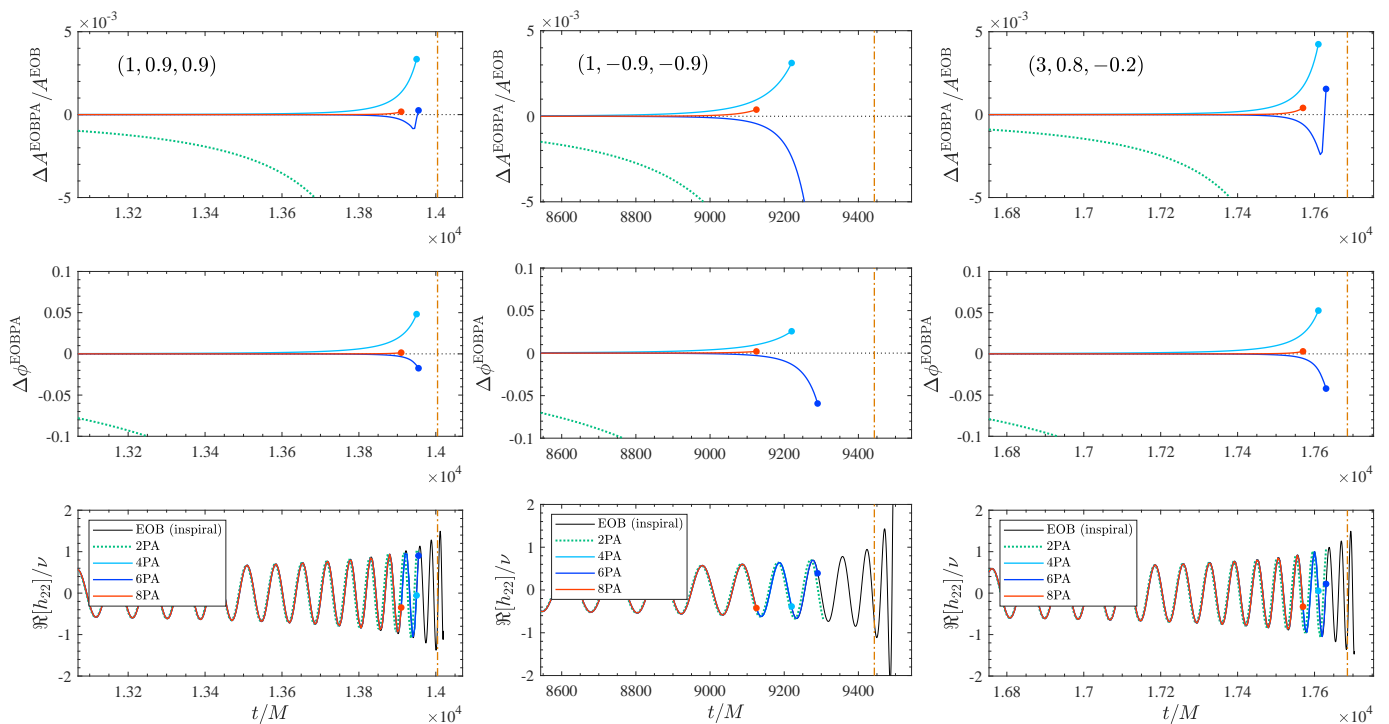


FIG. 11. Waveform comparison, $\ell = m = 2$ strain mode: EOB_{PA} inspiral (colours) versus EOB inspiral obtained solving the ODEs (black). Note that the waveform is the purely analytical EOB one and no merger and ringdown modelization is included. The orange vertical line marks the LSO crossing location on the time axis. The filled markers highlight the end of the PA inspirals.

waveform. The PA approximation is valid as long as the GW flux emitted by the binary is small. When this is no longer the case (typically a few orbits before merger), the PA approximation is used to generate the ODE initial conditions in order to compute the dynamics through plunge and merger.

Once we re-wrote the SEOBNRv4 Hamiltonian, we were able to repeat the procedure described in Ref. [28] for TEOBResumS. The model we tested is a hybrid, in that it uses the SEOBNRv4 conservative dynamics and the

TEOBResumS-like radiation reaction and waveform described in the previous section. This is clearly meant to be only a theoretical exercise to show the flexibility of the PA approach and it is not supposed to be, as is, faithful when compared with NR simulation data. The construction of the PA dynamics for SEOBNRv4 follows closely Ref. [28]. We alternately solve the two equations $dp_{r_*}/dt = (dp_{r_*}/dr)(dr/dt)$ and $dp_\varphi/dt = (dp_\varphi/dr)(dr/dt)$, in which we substitute Hamilton's equa-

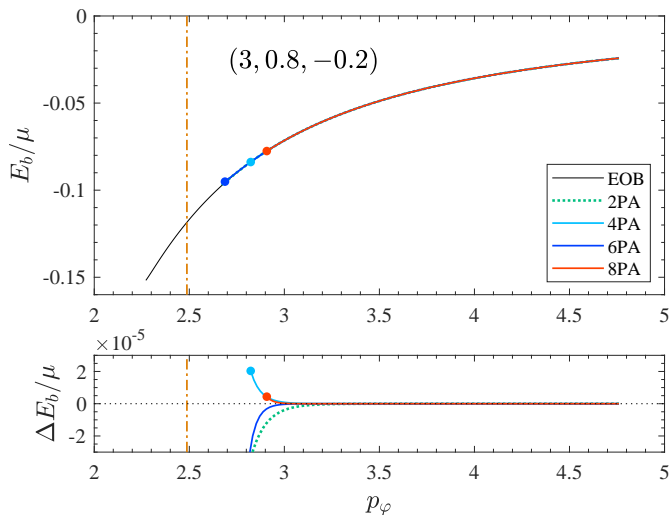


FIG. 12. Illustrative comparison between energies versus orbital angular momentum curves. The orange vertical line marks the EOB-LSO crossing.

tions, obtaining

$$\begin{aligned}
 & \left(\frac{\mathbb{A}}{\bar{r}_c^2} \right)' p_\varphi^2 + 2 \hat{\mathbb{H}}_{\text{eff}}^{\text{orb}} \left(\frac{\partial \tilde{\mathbb{G}}}{\partial r} + \frac{\partial \tilde{\mathbb{G}}}{\partial \bar{p}_{r_*}} \frac{d\bar{p}_{r_*}}{dr} \right) p_\varphi + \\
 & + \mathbb{A}' + z_3 \left(\frac{\mathbb{A}}{\bar{r}_c^2} \right)' \bar{p}_{r_*}^4 + 2 \left(1 + 2z_3 \frac{\mathbb{A}}{\bar{r}_c^2} \bar{p}_{r_*}^2 \right) \bar{p}_{r_*} \frac{d\bar{p}_{r_*}}{dr} + \\
 & + 2 \hat{\mathbb{H}}_{\text{eff}}^{\text{orb}} \left(\frac{\partial \hat{H}_{\text{SS}}^{\text{eff}}}{\partial r} + \frac{\partial \hat{H}_{\text{SS}}^{\text{eff}}}{\partial \bar{p}_{r_*}} \frac{d\bar{p}_{r_*}}{dr} \right) = 0, \quad (101) \\
 & \bar{p}_{r_*} = \hat{\mathcal{F}}_\varphi \left(\frac{dp_\varphi}{dr} \right)^{-1} \left(\frac{\mathbb{A}}{\mathbb{B}} \right)^{-1/2} \nu \hat{H}_{\text{EOB}} \hat{\mathbb{H}}_{\text{eff}}^{\text{orb}} \times \\
 & \times \left\{ 1 + 2z_3 \frac{\mathbb{A}}{\bar{r}_c^2} \bar{p}_{r_*}^2 + 2 \hat{\mathbb{H}}_{\text{eff}}^{\text{orb}} \left[p_\varphi \frac{\partial \tilde{\mathbb{G}}}{\partial (\bar{p}_{r_*}^2)} + \frac{\partial \hat{H}_{\text{SS}}^{\text{eff}}}{\partial (\bar{p}_{r_*}^2)} \right] \right\}^{-1}, \quad (102)
 \end{aligned}$$

where we defined

$$\tilde{\mathbb{G}} \equiv \bar{G}_S^0 \hat{S} + \mathbb{G}_{S_*} \hat{S}_* = \bar{G}_S \hat{S} + \bar{G}_{S_*} \hat{S}_*. \quad (103)$$

Equations (101) and (102) above translate Eqs. (5) and (6) of Ref. [28] into the SEOBnr4 dictionary, adding a term depending on $\hat{H}_{\text{SS}}^{\text{eff}}$, that is not present in TEObResumS. We denote as n PA order, the n -th iteration of this procedure, i.e. the n -th correction to the adiabatic momenta $(p_\varphi, p_{r_*}) = (p_\varphi^{\text{circ}}, 0)$. The accuracy of the PA approximation versus the standard ODE approach is illustrated in Figs. 11-12. While Fig. 11 compares the waveform phasing in different regions of the parameter space, Fig. 12 shows the gauge-invariant relation between binding energy and angular momentum. If, as expected, the 2PA order is far from being consistent with the ODE solution, the successive iterations rapidly converge to obtain a more than satisfying agreement. The 8PA order is consistent with the ODE up to the last three orbits before merger, as found in Ref. [28]. In the case of TEObResumS, this approach allowed for a drastic improvement of the waveform generation time (see Refs. [11, 29]). We have checked that this is the case also for the SEOBnr4 Hamiltonian *already* within a standard `Matlab` implementation analogous to

the one of Ref. [28], with comparable results. Currently, efforts are in progress so to implement the PA dynamics within the complete version of SEOBnr4 used by the LIGO-Virgo collaboration. Detailed results and timing comparisons will be presented in a forthcoming work.

VII. CONCLUSIONS

In this paper we have performed the first comprehensive analytic comparison between the Hamiltonians of the two state-of-the-art EOB waveform models for coalescing BBHs, TEObResumS and SEOBnr4. In particular, we have illustrated that the SEOBnr4 Hamiltonian can be *formally* written similarly to the TEObResumS one, though with different potentials. Generally speaking, this allowed us to illustrate that the most important structural differences between the two models lie in the way the ν -deformation is implemented in the spin sector. More precisely:

(i) *Centrifugal radius and spin-spin sector.* We have pointed out that in the orbital part of the SEOBnr4 Hamiltonian it is possible to identify a *centrifugal radius* function \bar{r}_c , similarly to r_c within TEObResumS. This function incorporates, in resummed form, some of the even-in-spin contribution, as in the case of a nonspinning particle on Kerr. However, \bar{r}_c and r_c are very different functions, notably because of the choice of the effective spin quantity. In particular, in TEObResumS the use of \tilde{a}_0 allows one to automatically incorporate within r_c the LO quadratic-in-spin (as well as quartic-in-spin) terms. This is not the case for SEOBnr4, that uses \hat{S} , so that a compensation term in the effective Hamiltonian, $\hat{H}_{\text{SS}}^{\text{eff}}$ has to be introduced. Another important difference comes from the fact that the resummation choices of SEOBnr4 include in \bar{r}_c the ν -dependent terms of Δ_u which are not present in TEObResumS.

(ii) *Spin-orbit sector.* We attempted to provide a one to one comparison between the spin-orbit sectors of the two models, rewriting the corresponding part of the SEOBnr4 Hamiltonian like the TEObResumS one. We identified the two gyro-gravitomagnetic functions $(\bar{G}_S, \bar{G}_{S_*})$ in the former that correspond to (G_S, G_{S_*}) in the latter. These functions differ both in the gauge choice and in the analytical content. We have explicitly showed that in SEOBnr4, the spin-orbit Hamiltonian can be obtained starting from the expression of Ref. [32] and ν -deforming it in some way, replacing the Kerr functions (r_c^K, A^K, B^K, Q^K) with $(\bar{r}_c, \mathbb{A}, \mathbb{B}, \mathbb{Q})$, that incorporate additional ν -dependent effects. From this point of view, we want to stress that most of the spinning-particle information that is encoded in $G_{S_*}^K$ is missing in TEObResumS, that is thus analytically *less complete* than SEOBnr4.

One should however be aware that nothing prevents us from the possibility of injecting the same information in an alternative Hamiltonian that, however, maintains the same global structure as the current one. In particular, the features that we want to preserve are: (i) the use of r_c with \tilde{a}_0 for spin-spin interaction and (ii) the use of factorized (and then

resummed) (G_S, G_{S_*}) function. In particular, one would like to keep for G_{S_*} a factorized expression of the form

$$G_{S_*} = G_{S_*}^0 \hat{G}_{S_*}, \quad (104)$$

where now $G_{S_*}^0$ reduces to $G_{S_*}^K$, Eq. (15), when $\nu = 0$ and *not* just to the first term of the PN expansion, $3/2 u^3$. To achieve this, one cannot work in the DJS gauge, but in a different gauge such that the standard PN-expanded G_{S_*} coincides with the Taylor expansion of $G_{S_*}^K$ when $\nu = 0$. One finds that this gauge is defined by the condition that all the ν -dependent terms that depend on the radial momentum disappear. The corresponding choice of the gauge parameters is reported at the end of Appendix E. A new spin-orbit sector that fully incorporates the spinning particle information can be obtained as follows: (i) one factorizes out from $g_{S_*}^{\text{eff}}$ the $r^3 G_{S_*}^K$ terms up to NNLO; (ii) $G_{S_*}^0$ is taken to have the same functional form of $G_{S_*}^K$ where, however, the various Kerr functions (r_c^K, A^K, B^K, Q^K) are replaced by the EOB ones, (r_c, A, B, Q) , with their complete ν -dependence. Similarly, the Kerr spin is replaced by the \tilde{a}_0 effective spin variable. The functions A and B are then resummed using the usual **TEOBResumS** prescriptions; finally, the new functions $(\hat{G}_S, \hat{G}_{S_*})$, that explicitly depend on ν , and are both in the form $1 + \dots$, are also resummed using their inverse Taylor representation, analogously to what is done in the DJS gauge. We found that incorporating the (ν -deformed) spinning-particle information within this new flavor of **TEOBResumS** fixes one of the long standing issues of the model in DJS gauge, i.e. the fact that the LSO does not exist for large, positive spins ≥ 0.7 , as recalled in the text and as pointed out in Ref. [41]. For this study, we also kept r_c at LO, i.e. setting $\delta a^2 = 0$ in Eq.(28), so to use the same amount of PN information as **SEOBNRv4**. Figure 13 shows the binding energy at the LSO obtained with this new model: one sees that the LSO always exists also for quasi-extremal, positive spins. We could also verify that, once implemented in the time-domain code to provide the full transition from early inspiral to plunge, merger and ringdown, the Hamiltonian in the new gauge maintains the same robustness and flexibility that was typical of the DJS gauge one. We also found that, analogously to this case, an effective spin-orbit parameter is necessary to get a good phasing agreement with NR simulations. A detailed investigation of these aspects is beyond the scope of this work and will be discussed elsewhere.

As last remarks, to make the comparison between the **SEOBNRv4** and **TEOBResumS** Hamiltonians more quantitative, we performed the following tasks.

- (a) We compared the gauge-invariant relations between energy, angular momentum and orbital frequency, both for adiabatic and nonadiabatic dynamics. In doing so, we compared and contrasted the linear-in-spin and quadratic-in-spin contributions of the two Hamiltonians. We found relevant qualitative and

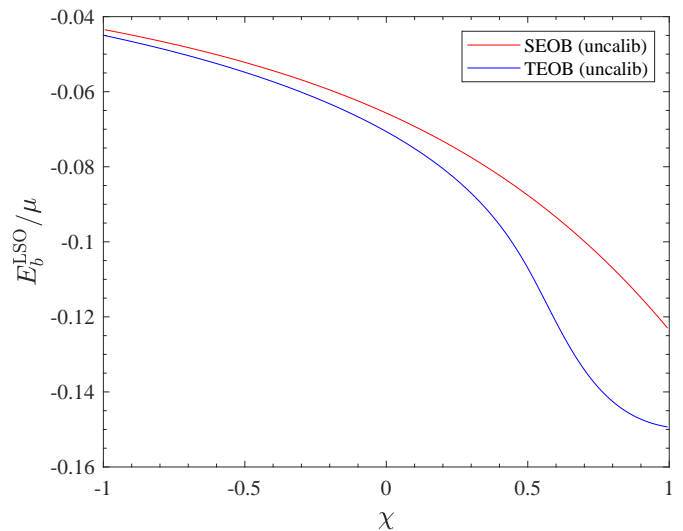


FIG. 13. Rescaled binding energy $\hat{E}_b \equiv E_b/\mu$ at the LSO for $q = 1$. This is obtained with the non-calibrated Hamiltonians of **SEOBNRv4** and **TEOBResumS**, where the latter includes a new G_{S_*} with the complete spinning particle information. Note that this new flavor of **TEOBResumS** presents an LSO for all values of the spin $\chi = \chi_1 = \chi_2$.

quantitative differences, especially in the spin-spin sector.

- (b) We proved the robustness of the **TEOBResumS** analytical framework by replacing the Padé resummed A -potential by the log-resummed A -potential used in **SEOBNRv4**. By a new NR-calibration of the K -function we constructed a new, *nonspinning* EOB model that is faithful ($\sim 10^{-3}$ level) with state-of-the-art NR simulations of the SXS catalog [42] and obtained with the BAM code, up to mass ratio $q = 18$.
- (c) Finally, we have illustrated that the post-adiabatic approximation introduced in Ref. [28] to efficiently generate long-inspiral waveforms can be implemented also using a **SEOBNRv4**-like Hamiltonian. Our result can thus be useful to improve the performance of the actual **SEOBNRv4** in its **LALInference** implementation, possibly avoiding the current need of building surrogate waveform models.

ACKNOWLEDGMENTS

D. B., P. R. and G. R. thank IHES for hospitality during the development of this work. We are grateful to R. Gamba for cross checking part of the analytical calculations. We thank A. Buonanno for comments on the manuscript.

Appendix A: Re-writing of the SEOBNRv4 Hamiltonian for generic spin orientations

In the main text we re-wrote the SEOBNRv4 Hamiltonian using the TEOBResumS formalism, once the former was restricted to equatorial orbits. This Appendix completes the discussion taking into account generic spin orientations.

1. Explicit calculation of \hat{H}_{NS}

In the generic case (with any value of θ), the metric components of Eqs. (46)–(50) read

$$g^{tt} = -\frac{\Lambda_t}{\Delta_t \Sigma}, \quad (\text{A1})$$

$$g^{rr} = \frac{\Delta_r}{\Sigma}, \quad (\text{A2})$$

$$g^{\theta\theta} = \frac{1}{\Sigma}, \quad (\text{A3})$$

$$g^{\varphi\varphi} = \frac{1}{\Lambda_t} \left(-\frac{\tilde{\omega}_{fd}^2}{\Delta_t \Sigma} + \frac{\Sigma}{\sin^2 \theta} \right), \quad (\text{A4})$$

$$g^{t\varphi} = -\frac{\tilde{\omega}_{fd}}{\Delta_t \Sigma}, \quad (\text{A5})$$

where

$$\Delta_t = r^2 \Delta_u, \quad (\text{A6})$$

$$\Delta_r = \Delta_t D^{-1}, \quad (\text{A7})$$

$$\Lambda_t = \left(r^2 + \hat{S}^2 \right)^2 - \hat{S}^2 \Delta_t \sin^2 \theta, \quad (\text{A8})$$

$$\Sigma = r^2 + \hat{S}^2 \cos^2 \theta, \quad (\text{A9})$$

$$\tilde{\omega}_{fd} = 2 \hat{S} r, \quad (\text{A10})$$

in which we already used the gauge freedom and imposed $\omega_{fd}^0 = \omega_{fd}^1 = 0$.

The “non-spinning” Hamiltonian \hat{H}_{NS} can then be computed using Eqs. (45) and substituting the newly defined functions.

At the same time, our rewriting of \hat{H}_{NS} , Eq. (62), still holds, when taking into account that the SEOBNRv4 metric potentials and centrifugal radius are again defined as

$$\bar{r}_c^2 \equiv \frac{\Lambda_t}{\Sigma}, \quad (\text{A11})$$

$$\mathbb{A} \equiv \frac{\Delta_t \Sigma}{\Lambda_t}, \quad (\text{A12})$$

$$\mathbb{B} \equiv \frac{\Sigma}{\Delta_r}, \quad (\text{A13})$$

$$\mathbb{Q} \equiv 1 + p_\varphi^2 \bar{u}_c^2 + \frac{p_{r^*}^2}{\mathbb{A}}, \quad (\text{A14})$$

$$\bar{G}_S^0 \equiv \frac{\tilde{\omega}_{fd}}{\Lambda_t \hat{S}}. \quad (\text{A15})$$

However, their explicit form is different and can be calculated using Eqs. (A6)–(A10). For example, the relation between the A and D function reads

$$\mathbb{D} = \frac{\bar{r}_c^2}{\Sigma} \mathbb{A} \mathbb{B}. \quad (\text{A16})$$

It is easily checked that we recover the equatorial orbits case for $\theta = \pi/2$.

2. Explicit calculation of \hat{H}_{SO}

In order to write the generic form of \hat{H}_{SO} , we first need to define some convention. We indicate with \mathbf{r} and \mathbf{p} the dimensionless position and momentum vectors respectively. The spin vectors corresponding to the variables of Eqs. (74)–(75) are denoted by $\vec{\mathcal{S}}$ and $\vec{\mathcal{S}}_*$. Using this notation, the general form of \hat{H}_{SO} , given by Eq. (4.18) of Ref. [19], reads

$$\begin{aligned} \hat{H}_{\text{SO}} = & (\mathbf{p} \cdot \boldsymbol{\xi} r) \left(\vec{\mathcal{S}}_* \cdot \mathbf{s} \right) \frac{e^{2\tilde{\nu}-\tilde{\mu}} \left(e^{\tilde{\mu}+\tilde{\nu}} - \tilde{B} \right)}{\tilde{B}^2 \sqrt{\mathbb{Q}} \xi^2} + \frac{e^{\tilde{\nu}-2\tilde{\mu}}}{\tilde{B}^2 (1 + \sqrt{\mathbb{Q}}) \sqrt{\mathbb{Q}} \xi^2} \left\{ \tilde{B}^2 \tilde{J} \left[\left(\tilde{\mu}' - \frac{1}{\tilde{J}} \right) (\mathbf{p} \cdot \mathbf{v} r) (1 + \sqrt{\mathbb{Q}}) + \right. \right. \\ & \left. \left. - \partial_{\cos \theta} (\tilde{\mu}) (\mathbf{p} \cdot \mathbf{n}) \xi^2 - \sqrt{\mathbb{Q}} (\tilde{\nu}' (\mathbf{p} \cdot \mathbf{v} r) + \partial_{\cos \theta} (\tilde{\mu} - \tilde{\nu}) (\mathbf{p} \cdot \mathbf{n}) \xi^2) \right] \left(\vec{\mathcal{S}}_* \cdot \boldsymbol{\xi} \right) + \right. \\ & \left. + e^{\tilde{\mu}+\tilde{\nu}} (\mathbf{p} \cdot \boldsymbol{\xi} r) \left(2\sqrt{\mathbb{Q}} + 1 \right) \left[\tilde{J} \tilde{\nu}' \left(\vec{\mathcal{S}}_* \cdot \mathbf{v} \right) - \partial_{\cos \theta} (\tilde{\nu}) \xi^2 \left(\vec{\mathcal{S}}_* \cdot \mathbf{n} \right) \right] \tilde{B} + \right. \\ & \left. - \tilde{J} \left(\tilde{B}' - \frac{\tilde{B}}{\tilde{J}} \right) e^{\tilde{\mu}+\tilde{\nu}} (\mathbf{p} \cdot \boldsymbol{\xi} r) (1 + \sqrt{\mathbb{Q}}) \left(\vec{\mathcal{S}}_* \cdot \mathbf{v} \right) \right\}, \quad (\text{A17}) \end{aligned}$$

where the used unit vectors are $\mathbf{n} = \mathbf{r}/r$, $\mathbf{s} = \vec{\mathcal{S}}/|\vec{\mathcal{S}}|$, $\boldsymbol{\xi} = \mathbf{s} \times \mathbf{n}$ and $\mathbf{v} = \mathbf{n} \times \boldsymbol{\xi}$.

still formally read

$$e^{2\tilde{\mu}} = \Sigma, \quad e^{2\tilde{\nu}} = \frac{\Delta_t \Sigma}{\Lambda_t}, \quad (\text{A18})$$

$$\tilde{B} = \sqrt{\Delta_t}, \quad \tilde{J} = \sqrt{\Delta_r}, \quad (\text{A19})$$

The functions that enter the “spin-orbit” Hamiltonian

but are related to the TEOBResumS-like functions by

$$e^{2\bar{\mu}} = \Sigma, \quad e^{2\bar{\nu}} = \mathbb{A}, \quad (\text{A20})$$

$$\tilde{B} = \sqrt{\mathbb{A}} \bar{r}_c, \quad \tilde{J} = \frac{\sqrt{\Sigma}}{\sqrt{\mathbb{B}}}. \quad (\text{A21})$$

Substituting these formulas into Eq. (A17), we get

$$\begin{aligned} \hat{H}_{\text{SO}} = & \frac{\sqrt{\mathbb{A}}}{\sqrt{\mathbb{Q}} \xi^2} \frac{\sqrt{\Sigma} - \bar{r}_c}{\bar{r}_c^2 \sqrt{\Sigma}} (\mathbf{p} \cdot \boldsymbol{\xi} r) (\vec{\mathbb{S}}_* \cdot \mathbf{s}) + \frac{\sqrt{\mathbb{A}}}{\sqrt{\mathbb{B}} \bar{r}_c \xi^2} \left[\frac{\mathbb{A}'}{2(1+\sqrt{\mathbb{Q}}) \mathbb{A}} - \frac{(\bar{r}_c)'}{\sqrt{\mathbb{Q}} \bar{r}_c} + \frac{\sqrt{\mathbb{B}}}{\sqrt{\mathbb{Q}} \sqrt{\Sigma}} \right] (\mathbf{p} \cdot \boldsymbol{\xi} r) (\vec{\mathbb{S}}_* \cdot \mathbf{v}) + \\ & + \frac{1}{2\sqrt{\mathbb{A}} \sqrt{\mathbb{B}} \sqrt{\Sigma}} \left\{ \left[\frac{\partial_{\cos \theta} \mathbb{A}}{1+\sqrt{\mathbb{Q}}} - \frac{\mathbb{A}}{\sqrt{\mathbb{Q}}} \frac{\partial_{\cos \theta} \Sigma}{\Sigma} \right] (\mathbf{p} \cdot \mathbf{n}) - \frac{1}{\xi^2} \left[\frac{\mathbb{A}'}{(1+\sqrt{\mathbb{Q}})} - \frac{\mathbb{A}}{\sqrt{\mathbb{Q}}} \frac{(\Sigma)'}{\Sigma} - 2\sqrt{\mathbb{B}} \sqrt{\Sigma} \right] (\mathbf{p} \cdot \mathbf{v} r) \right\} (\vec{\mathbb{S}}_* \cdot \boldsymbol{\xi}) + \\ & - \frac{1+2\sqrt{\mathbb{Q}}}{2\sqrt{\mathbb{Q}}(1+\sqrt{\mathbb{Q}})} \frac{\partial_{\cos \theta} \mathbb{A}}{\sqrt{\Sigma} \sqrt{\mathbb{A}} \bar{r}_c} (\mathbf{p} \cdot \boldsymbol{\xi} r) (\vec{\mathbb{S}}_* \cdot \mathbf{n}). \end{aligned} \quad (\text{A22})$$

In the spin-aligned case, we find $(\vec{\mathbb{S}}_* \cdot \boldsymbol{\xi}) = (\vec{\mathbb{S}}_* \cdot \mathbf{n}) = 0$ and $(\vec{\mathbb{S}}_* \cdot \mathbf{v}) = (\vec{\mathbb{S}}_* \cdot \mathbf{s}) = \hat{S}_*$. We also define the radial and angular momentum as $(\mathbf{p} \cdot \mathbf{n}) = p_r$ and $(\mathbf{p} \cdot \boldsymbol{\xi} r) = p_\varphi$ respectively, while $(\mathbf{p} \cdot \mathbf{v} r) = 0$. Finally, we fix $\theta = \pi/2$, such that $\xi^2 = 1$.

3. Explicit calculation of \hat{H}_{SS}

Let us turn now to the function $\hat{H}_{\text{SS}}^{\text{eff}}$. Following Eq. (4.19) of Ref. [19] we write

$$\begin{aligned} \hat{H}_{\text{SS}} = & \omega (\vec{\mathbb{S}}_* \cdot \mathbf{s}) + \frac{e^{-3\bar{\mu}-\bar{\nu}} \tilde{J}}{2\tilde{B} \xi^2} \frac{\omega'}{\sqrt{\mathbb{Q}}(1+\sqrt{\mathbb{Q}})} \left\{ -e^{\bar{\nu}+\bar{\mu}} (\mathbf{p} \cdot \mathbf{v} r) (\mathbf{p} \cdot \boldsymbol{\xi} r) (\vec{\mathbb{S}}_* \cdot \boldsymbol{\xi}) \tilde{B} + e^{2(\bar{\nu}+\bar{\mu})} (\mathbf{p} \cdot \boldsymbol{\xi} r)^2 (\vec{\mathbb{S}}_* \cdot \mathbf{v}) + \right. \\ & + e^{2\bar{\mu}} (1+\sqrt{\mathbb{Q}}) \sqrt{\mathbb{Q}} (\vec{\mathbb{S}}_* \cdot \mathbf{v}) \xi^2 \tilde{B}^2 + \tilde{J} (\mathbf{p} \cdot \mathbf{n}) \left[(\mathbf{p} \cdot \mathbf{v} r) (\vec{\mathbb{S}}_* \cdot \mathbf{n}) - \tilde{J} (\mathbf{p} \cdot \mathbf{n}) (\vec{\mathbb{S}}_* \cdot \mathbf{v}) \right] \xi^2 \tilde{B}^2 \left. \right\} + \\ & + \frac{e^{-3\bar{\mu}-\bar{\nu}} \partial_{\cos \theta} (\omega)}{2\tilde{B} \sqrt{\mathbb{Q}} (1+\sqrt{\mathbb{Q}})} \left\{ -e^{2(\bar{\mu}+\bar{\nu})} (\mathbf{p} \cdot \boldsymbol{\xi} r)^2 (\vec{\mathbb{S}}_* \cdot \mathbf{n}) + e^{\bar{\mu}+\bar{\nu}} \tilde{J} \tilde{B} (\mathbf{p} \cdot \mathbf{n}) (\mathbf{p} \cdot \boldsymbol{\xi} r) (\vec{\mathbb{S}}_* \cdot \boldsymbol{\xi}) + \right. \\ & \left. + \tilde{B}^2 \left[(\vec{\mathbb{S}}_* \cdot \mathbf{n}) (\mathbf{p} \cdot \mathbf{v} r)^2 - \tilde{J} (\mathbf{p} \cdot \mathbf{n}) (\mathbf{p} \cdot \mathbf{v} r) (\vec{\mathbb{S}}_* \cdot \mathbf{v}) - e^{2\bar{\mu}} (1+\sqrt{\mathbb{Q}}) \sqrt{\mathbb{Q}} \xi^2 (\vec{\mathbb{S}}_* \cdot \mathbf{n}) \right] \right\}, \end{aligned} \quad (\text{A23})$$

where again

$$\omega \equiv \frac{\tilde{\omega}_{fd}}{\Lambda_t} = \bar{G}_S^0 \hat{S}. \quad (\text{A24})$$

Eq. (A23) then becomes

$$\begin{aligned} \hat{H}_{\text{SS}} = & \bar{G}_S^0 \hat{S} (\vec{\mathbb{S}}_* \cdot \mathbf{s}) + \frac{\bar{r}_c}{2\xi^2 \sqrt{\mathbb{B}}} (\bar{G}_S^0)' \hat{S} \left\{ \xi^2 (\vec{\mathbb{S}}_* \cdot \mathbf{v}) + \frac{1}{\sqrt{\mathbb{Q}}(1+\sqrt{\mathbb{Q}})} \times \right. \\ & \times \left[\left(\frac{(\mathbf{p} \cdot \boldsymbol{\xi} r)^2}{\bar{r}_c^2} - \frac{\xi^2 (\mathbf{p} \cdot \mathbf{n})^2}{\mathbb{B}} \right) (\vec{\mathbb{S}}_* \cdot \mathbf{v}) - \frac{(\mathbf{p} \cdot \boldsymbol{\xi} r) (\mathbf{p} \cdot \mathbf{v} r)}{\sqrt{\Sigma} \bar{r}_c} (\vec{\mathbb{S}}_* \cdot \boldsymbol{\xi}) + \frac{\xi^2 (\mathbf{p} \cdot \mathbf{n}) (\mathbf{p} \cdot \mathbf{v} r)}{\sqrt{\mathbb{B}} \sqrt{\Sigma}} (\vec{\mathbb{S}}_* \cdot \mathbf{n}) \right] \left. \right\} + \\ & - \frac{\bar{r}_c}{2\sqrt{\Sigma}} \partial_{\cos \theta} (\bar{G}_S^0) \hat{S} \left\{ \xi^2 (\vec{\mathbb{S}}_* \cdot \mathbf{n}) + \frac{1}{\sqrt{\mathbb{Q}}(1+\sqrt{\mathbb{Q}})} \times \right. \\ & \times \left[\left(\frac{(\mathbf{p} \cdot \boldsymbol{\xi} r)^2}{\bar{r}_c^2} - \frac{(\mathbf{p} \cdot \mathbf{v} r)^2}{\Sigma} \right) (\vec{\mathbb{S}}_* \cdot \mathbf{n}) - \frac{(\mathbf{p} \cdot \boldsymbol{\xi} r) (\mathbf{p} \cdot \mathbf{n})}{\sqrt{\mathbb{B}} \bar{r}_c} (\vec{\mathbb{S}}_* \cdot \boldsymbol{\xi}) + \frac{(\mathbf{p} \cdot \mathbf{n}) (\mathbf{p} \cdot \mathbf{v} r)}{\sqrt{\mathbb{B}} \sqrt{\Sigma}} (\vec{\mathbb{S}}_* \cdot \mathbf{v}) \right] \left. \right\}. \end{aligned} \quad (\text{A25})$$

Finally, the total $\hat{H}_{\text{SS}}^{\text{eff}}$, without NR calibration, is defined as

$$\hat{H}_{\text{SS}}^{\text{eff}} = \hat{H}_{\text{SS}} - \frac{1}{2}u^3 (\delta_{ij} - n_i n_j) \hat{S}_*^i \hat{S}_*^j. \quad (\text{A26})$$

To go back to the spin-aligned case, we impose the conditions described in the previous section.

Appendix B: PN coefficients in G_S and G_{S^*}

We write here explicitly the coefficients that enter Eqs. (37) and (38). They are

$$\begin{aligned} c_{10} &= \frac{5}{16}\nu, & c_{10}^* &= \frac{3}{4} + \frac{1}{2}\nu, \\ c_{20} &= \frac{51}{8}\nu + \frac{41}{256}\nu^2, & c_{20}^* &= \frac{27}{16} + \frac{29}{4}\nu + \frac{3}{8}\nu^2, \\ c_{30} &= \nu c_3, & c_{30}^* &= \frac{135}{32} + \nu c_3, \\ c_{12} &= 12\nu - \frac{49}{128}\nu^2, & c_{12}^* &= 4 + 11\nu - \frac{7}{8}\nu^2, \\ c_{02} &= \frac{27}{16}\nu, & c_{02}^* &= \frac{5}{84} + \frac{3}{2}\nu, \\ c_{04} &= -\frac{5}{16}\nu + \frac{169}{256}\nu^2, & c_{04}^* &= \frac{5}{48} + \frac{25}{12}\nu + \frac{3}{8}\nu^2, \\ & & c_{40}^* &= \frac{2835}{256}, \end{aligned} \quad (\text{B1})$$

Appendix C: Coefficients of the Δ_u function

We list here the explicit expression of the (Δ_0, Δ_i) coefficients used in the log-resummation of the potential in SEOBNRv4 in Eq. (59). They read

$$\Delta_0 = K(K\nu - 2), \quad (\text{C1})$$

$$\Delta_1 = -2(\Delta_0 + K)(K\nu - 1), \quad (\text{C2})$$

$$\Delta_2 = \frac{1}{2}(\Delta_1(\Delta_1 - 4K\nu + 4) - 2a^2\Delta_0(K\nu - 1)^2), \quad (\text{C3})$$

$$\Delta_3 = -a^2\Delta_1(K\nu - 1)^2 - \frac{\Delta_1^3}{3} + \Delta_1^2(K\nu - 1) + \Delta_1\Delta_2 - 2(K\nu - 1)(\Delta_2 - K\nu + 1), \quad (\text{C4})$$

$$\begin{aligned} \Delta_4 &= \frac{1}{96} \left[8(6a^2(\Delta_1^2 - 2\Delta_2)(K\nu - 1)^2 + 3\Delta_1^4 + \Delta_1^3(8 - 8K\nu) - 12\Delta_1^2\Delta_2 + 12\Delta_1(2\Delta_2K\nu - 2\Delta_2 + \Delta_3)) \right. \\ &\quad \left. + 48\Delta_2^2 - 64(K\nu - 1)(3\Delta_3 - 47K\nu + 47) - 123\pi^2(K\nu - 1)^2 \right], \end{aligned} \quad (\text{C5})$$

$$\begin{aligned} \Delta_5 &= \frac{(K\nu - 1)^2}{\nu} \left[\frac{64}{5}\nu \log(u) + \nu \left(-\frac{1}{3}a^2(\Delta_1^3 - 3\Delta_1\Delta_2 + 3\Delta_3) + \frac{\Delta_1^4 - 4\Delta_1^2\Delta_2 + 4\Delta_1\Delta_3 + 2\Delta_2^2 - 4\Delta_4}{2K\nu - 2} \right. \right. \\ &\quad \left. \left. - \frac{\Delta_1^5 - 5\Delta_1^3\Delta_2 + 5\Delta_1^2\Delta_3 + 5\Delta_1\Delta_2^2 - 5\Delta_2\Delta_3 - 5\Delta_4\Delta_1}{5(K\nu - 1)^2} + \frac{2275\pi^2}{512} + \frac{128\gamma}{5} - \frac{4237}{60} + \frac{256 \log(2)}{5} \right) \right. \\ &\quad \left. + \left(\frac{41}{32}\pi^2 - \frac{221}{6} \right) \nu^2 \right]. \end{aligned} \quad (\text{C6})$$

Appendix D: Re-writing of the spin mapping of \hat{S}_*

In this Appendix we show the explicit form of the coefficients that enter the spin mapping of Eq. (75).

Comparing Eqs. (81) and (82) with Eqs. (51) and (52)

of Ref. [21], we get

$$c_u = \frac{1}{6}(-4b_0 + 7\nu)\hat{S} - \frac{2}{3}(a_0 + \nu)\hat{S}_*, \quad (\text{D1})$$

$$c_Q = \frac{1}{3}(2b_0 + \nu) + \frac{1}{12}(8a_0 + 3\nu)\hat{S}_*, \quad (\text{D2})$$

$$c_{pr^2} = -\frac{1}{2}(4b_0 + 5\nu) - (2a_0 + 3\nu)\hat{S}_*, \quad (\text{D3})$$

and

$$c_u^2 = \frac{1}{36} (-56b_0 - 24b_2 + 353\nu - 60b_0\nu - 27\nu^2) \hat{S} + \frac{1}{9} (-14a_0 - 6a_2 - 56\nu - 15a_0\nu - 21\nu^2) \hat{S}_*, \quad (\text{D4})$$

$$c_{\mathbb{Q}^2} = \frac{1}{72} (-4b_0 + 48b_1 - 23\nu - 12b_0\nu - 3\nu^2) \hat{S} + \frac{1}{144} (-8a_0 + 96a_1 - 45\nu - 24a_0\nu) \hat{S}_*, \quad (\text{D5})$$

$$c_{u\mathbb{Q}} = \frac{1}{36} (-14b_0 - 24b_1 + 24b_2 - 103\nu + 66b_0\nu + 60\nu^2) \hat{S} + \frac{1}{36} (-14a_0 - 24a_1 + 24a_2 - 109\nu + 66a_0\nu + 51\nu^2) \hat{S}_*, \quad (\text{D6})$$

$$c_{p_r^4} = \frac{5}{3} (-2b_3 + 3b_0\nu + 3\nu^2) \hat{S} + \frac{5}{24} (-16a_3 + 24a_0\nu + 27\nu^2) \hat{S}_*, \quad (\text{D7})$$

$$c_{up_r^2} = \frac{1}{12} (-24b_0 - 16b_1 - 32b_2 - 24b_3 + 43\nu - 24b_0\nu - 54\nu^2) \hat{S} + \frac{1}{24} (-48a_0 - 36a_1 + 64a_2 - 48a_3 - 16\nu - 48a_0\nu - 147\nu^2) \hat{S}_*, \quad (\text{D8})$$

$$c_{p_r^2\mathbb{Q}} = \frac{1}{12} (2b_0 - 24b_1 + 24b_3 + 16\nu - 30b_0\nu - 21\nu^2) \hat{S} + \frac{1}{24} (4a_0 - 48a_1 + 48a_3 + 6\nu - 60a_0\nu - 39\nu^2) \hat{S}_*. \quad (\text{D9})$$

If we now decide to extract the spin dependence, we can write

$$\Delta_{\sigma^*}^{(1)} = c_S^{(1)} \hat{S} + c_{S^*}^{(1)} \hat{S}_*, \quad (\text{D10})$$

$$\Delta_{\sigma^*}^{(2)} = c_S^{(2)} \hat{S} + c_{S^*}^{(2)} \hat{S}_*, \quad (\text{D11})$$

where the coefficients $(c_S^{(i)}, c_{S^*}^{(i)})$ now are independent of spins, but depend on dynamical variables. These, with their complete gauge flexibility, read

$$c_S^{(1)} = \frac{2}{3} u (a_0 + \nu) + \frac{1}{12} (8a_0 + 3\nu) (\mathbb{Q} - 1) - (2a_0 + 3\nu) \frac{p_r^2}{\mathbb{B}}, \quad (\text{D12})$$

$$c_{S^*}^{(1)} = \frac{1}{6} u (-4b_0 + 7\nu) + \frac{1}{3} (\mathbb{Q} - 1) (2b_0 + \nu) - \frac{1}{2} \frac{p_r^2}{\mathbb{B}} (4b_0 + 5\nu), \quad (\text{D13})$$

and

$$c_S^{(2)} = \frac{1}{9} u^2 (-14a_0 - 6a_2 - 56\nu - 15a_0\nu - 21\nu^2) + \frac{5}{24} \frac{p_r^4}{\mathbb{B}^2} (-16a_3 + 24a_0\nu + 27\nu^2) + \frac{1}{144} (\mathbb{Q} - 1)^2 (-8a_0 + 96a_1 - 45\nu - 24a_0\nu) + \frac{1}{36} u (\mathbb{Q} - 1) (-14a_0 - 24a_1 + 24a_2 - 109\nu + 66a_0\nu + 51\nu^2) + \frac{1}{24} (\mathbb{Q} - 1) \frac{p_r^2}{\mathbb{B}} (4a_0 - 48a_1 + 48a_3 + 6\nu - 60a_0\nu - 39\nu^2) + \frac{1}{24} u \frac{p_r^2}{\mathbb{B}} (-48a_0 - 32a_1 + 64a_2 - 48a_3 - 16\nu - 48a_0\nu - 147\nu^2), \quad (\text{D14})$$

$$c_{S^*}^{(2)} = \frac{1}{36} u^2 (-56b_0 - 24b_2 + 353\nu - 60b_0\nu - 27\nu^2) + \frac{5}{3} \frac{p_r^4}{\mathbb{B}^2} (-2b_3 + 3b_0\nu + 3\nu^2) + \frac{1}{72} (\mathbb{Q} - 1)^2 (-4b_0 + 48b_1 - 23\nu - 12b_0\nu - 3\nu^2) + \frac{1}{36} u (\mathbb{Q} - 1) (-14b_0 - 24b_1 + 24b_2 - 103\nu + 66b_0\nu + 60\nu^2) + \frac{1}{12} (\mathbb{Q} - 1) \frac{p_r^2}{\mathbb{B}} (2b_0 - 24b_1 + 24b_3 + 16\nu - 30b_0\nu - 21\nu^2) + \frac{1}{12} u \frac{p_r^2}{\mathbb{B}} (-24b_0 - 16b_1 - 32b_2 + 24b_3 + 47\nu - 24b_0\nu - 54\nu^2). \quad (\text{D15})$$

Applying the `SEOBNRv4` gauge choice ($a_i = b_i = 0$), the former coefficients become

$$c_S^{(1)} = \frac{\nu}{4} (\mathbb{Q} - 1) + \frac{2}{3} u\nu, \quad (\text{D16})$$

$$c_S^{(2)} = -\frac{5}{16} \nu (\mathbb{Q} - 1)^2 + \frac{1}{36} (51\nu^2 - 109\nu) (\mathbb{Q} - 1) u + \frac{1}{9} (-21\nu^2 - 56\nu) u^2, \quad (\text{D17})$$

and

$$c_{S^*}^{(1)} = \frac{1}{3} \nu (\mathbb{Q} - 1) + \frac{7\nu u}{6}, \quad (\text{D18})$$

$$c_{S^*}^{(2)} = \frac{1}{72} (-3\nu^2 - 23\nu) (\mathbb{Q} - 1)^2 + \frac{1}{36} (60\nu^2 - 103\nu) (\mathbb{Q} - 1) u + \frac{1}{36} (353\nu - 27\nu^2) u^2. \quad (\text{D19})$$

Appendix E: Gauge fixings

We here report explicitly the connection between the spin gauges used in the spin-orbit sectors of the two models. We recall that `TEOBResumS` makes use of the `DJS` gauge, while `SEOBNRv4` sets all gauge parameters to zero.

Let us list here the explicit gauge choices on the PN-expanded gyro-gravitomagnetic ratios [30] $g_S^{\text{eff}} \equiv r^3 G_S$ and $g_{S^*}^{\text{eff}} \equiv r^3 G_{S^*}$. At NNLO level they read

$$g_S^{\text{eff}} = 2 + \frac{1}{c^2} g_S^{\text{effNLO}} + \frac{1}{c^4} g_S^{\text{effNNLO}}, \quad (\text{E1})$$

$$g_{S^*}^{\text{eff}} = \frac{3}{2} + \frac{1}{c^2} g_{S^*}^{\text{effNLO}} + \frac{1}{c^4} g_{S^*}^{\text{effNNLO}},$$

where the NLO terms read

$$g_S^{\text{effNLO}} = \left(\left(\frac{3}{8}\nu + a \right) \mathbf{p}^2 + \left(\frac{9}{2}\nu + 3a \right) (\mathbf{p} \cdot \mathbf{n})^2 - u(\nu + a) \right), \quad (\text{E2})$$

$$g_{S_*}^{\text{effNLO}} = \left(-\frac{5}{8} + \frac{\nu}{2} + b \right) \mathbf{p}^2 + \left(\frac{15}{4}\nu + 3b \right) (\mathbf{p} \cdot \mathbf{n})^2 - u \left(\frac{1}{2} + \frac{5}{4}\nu + b \right), \quad (\text{E3})$$

and the NNLO ones are expressed as

$$g_S^{\text{effNNLO}} = -u^2 \left(9\nu + \frac{3}{2}\nu^2 + a + \alpha \right) + u \left[(\mathbf{p} \cdot \mathbf{n})^2 \left(\frac{35}{4}\nu - \frac{3}{16}\nu^2 + 6a - 4\alpha - 3\beta - 2\gamma \right) + \mathbf{p}^2 \left(-\frac{17}{4}\nu + \frac{11}{8}\nu^2 - \frac{3}{2}a + \alpha - \gamma \right) \right] + \left(\frac{9}{4}\nu - \frac{39}{16}\nu^2 + \frac{3}{2}a + 3\beta - 3\gamma \right) \mathbf{p}^2 (\mathbf{p} \cdot \mathbf{n})^2 + \left(\frac{135}{16}\nu^2 - 5\beta \right) (\mathbf{p} \cdot \mathbf{n})^4 + \left(-\frac{5}{8}\nu - \frac{a}{2} + \gamma \right) \mathbf{p}^4, \quad (\text{E4})$$

$$g_{S_*}^{\text{effNNLO}} = -u^2 \left(\frac{1}{2} + \frac{55}{8}\nu + \frac{13}{8}\nu^2 + b + \delta \right) + u \left[\mathbf{p}^2 \left(\frac{1}{4} - \frac{59}{16}\nu + \frac{3}{2}\nu^2 - \frac{3}{2}b + \delta - \eta \right) + (\mathbf{p} \cdot \mathbf{n})^2 \left(\frac{5}{4} + \frac{109}{8}\nu + \frac{3}{4}\nu^2 + 6b - 4\delta - 3\zeta - 2\eta \right) \right] + \left(\frac{57}{16}\nu - \frac{21}{8}\nu^2 + \frac{3}{2}b + 3\zeta - 3\eta \right) \mathbf{p}^2 (\mathbf{p} \cdot \mathbf{n})^2 + \left(\frac{15}{2}\nu^2 - 5\zeta \right) (\mathbf{p} \cdot \mathbf{n})^4 + \left(\frac{7}{16} - \frac{11}{16}\nu - \frac{\nu^2}{16} - \frac{b}{2} + \eta \right) \mathbf{p}^4. \quad (\text{E5})$$

The DJS gauge used within `TEOBResumS` is defined by

$$\begin{aligned} a &= -\frac{3}{8}\nu, & b &= \frac{5}{8} - \frac{\nu}{2}, \\ \alpha &= \frac{11}{8}\nu(3 - \nu), & \beta &= \frac{\nu}{16}(13\nu - 2), \\ \gamma &= \frac{7}{16}\nu, & \delta &= \frac{1}{16}(9 + 54\nu - 23\nu^2), \\ \zeta &= \frac{1}{16}(-7 - 8\nu + 15\nu^2), & \eta &= \frac{1}{16}(-2 + 7\nu + \nu^2). \end{aligned} \quad (\text{E6})$$

By contrast, the gauge chosen for `SEOBNRv4` is defined by imposing $a_i = b_i = 0$ with $i = (0, 1, 2, 3)$, as pointed out in Ref. [22]. The gauge parameters (a_i, b_i) (see Eqs. (51) and (52) therein) are related to the former ones by

$$\begin{aligned} a_0 &= a, & a_1 &= \gamma + \frac{\nu}{4}a, \\ a_2 &= \alpha - a \left(1 + \frac{\nu}{2} \right), & a_3 &= \beta + \frac{3}{2}a\nu, \\ b_0 &= b, & b_1 &= \eta + \frac{\nu}{4}b, \\ b_2 &= \delta - b \left(1 + \frac{\nu}{2} \right), & b_3 &= \zeta + \frac{3}{2}\nu b. \end{aligned} \quad (\text{E7})$$

1. Gauge-fixing for the new `TEOBResumS` G_{S_*}

In order to include the complete Hamiltonian of a spinning particle on a Kerr background within `TEOBResumS`, we cannot use the DJS gauge. Instead we need to work in a gauge such that the PN-expanded G_{S_*} coincides with the Taylor expansion of $G_{S_*}^K$ when $\nu \rightarrow 0$. This gauge is defined by the condition that all the ν -dependent terms that depend on $(\mathbf{n} \cdot \mathbf{p})$ disappear. The corresponding choice of the gauge parameters in $(g_S^{\text{eff}}, g_{S_*}^{\text{eff}})$ is then

$$\begin{aligned} a &= -\frac{3}{2}\nu, & b &= -\frac{5}{4}\nu, \\ \alpha &= -\frac{\nu}{16}(1 + 28\nu), & \beta &= \frac{27}{16}\nu^2, \\ \gamma &= \frac{7}{8}\nu^2, & \delta &= \frac{5}{4}\nu(1 - \nu), \\ \zeta &= \frac{3}{2}\nu^2, & \eta &= \frac{\nu}{16}(9 + 10\nu). \end{aligned} \quad (\text{E8})$$

-
- [1] B. P. Abbott et al. (LIGO Scientific, Virgo), (2018), [arXiv:1811.12907](https://arxiv.org/abs/1811.12907) [astro-ph.HE].
- [2] A. Buonanno and T. Damour, *Phys. Rev.* **D59**, 084006 (1999), [arXiv:gr-qc/9811091](https://arxiv.org/abs/gr-qc/9811091).
- [3] A. Buonanno and T. Damour, *Phys. Rev.* **D62**, 064015 (2000), [arXiv:gr-qc/0001013](https://arxiv.org/abs/gr-qc/0001013).
- [4] T. Damour, P. Jaranowski, and G. Schaefer, *Phys. Rev.* **D62**, 084011 (2000), [arXiv:gr-qc/0005034](https://arxiv.org/abs/gr-qc/0005034) [gr-qc].
- [5] T. Damour, B. R. Iyer, and A. Nagar, *Phys. Rev.* **D79**, 064004 (2009), [arXiv:0811.2069](https://arxiv.org/abs/0811.2069) [gr-qc].
- [6] L. Blanchet, *Living Rev. Relativity* **17**, 2 (2014), [arXiv:1310.1528](https://arxiv.org/abs/1310.1528) [gr-qc].
- [7] G. Schaefer and P. Jaranowski, *Living Rev. Rel.* **21**, 7 (2018), [arXiv:1805.07240](https://arxiv.org/abs/1805.07240) [gr-qc].
- [8] A. Bohé et al., *Phys. Rev.* **D95**, 044028 (2017), [arXiv:1611.03703](https://arxiv.org/abs/1611.03703) [gr-qc].
- [9] R. Cotesta, A. Buonanno, A. Bohé, A. Taracchini, I. Hinder, and S. Ossokine, *Phys. Rev.* **D98**, 084028 (2018), [arXiv:1803.10701](https://arxiv.org/abs/1803.10701) [gr-qc].
- [10] A. Nagar et al., *Phys. Rev.* **D98**, 104052 (2018), [arXiv:1806.01772](https://arxiv.org/abs/1806.01772) [gr-qc].
- [11] A. Nagar, F. Messina, P. Rettegno, D. Bini, T. Damour, A. Geralico, S. Akcay, and S. Bernuzzi, *Phys. Rev.* **D99**, 044007 (2019), [arXiv:1812.07923](https://arxiv.org/abs/1812.07923) [gr-qc].
- [12] Y. Pan, A. Buonanno, A. Taracchini, L. E. Kidder, A. H. Mroue, et al., *Phys. Rev.* **D89**, 084006 (2014), [arXiv:1307.6232](https://arxiv.org/abs/1307.6232) [gr-qc].
- [13] S. Babak, A. Taracchini, and A. Buonanno, *Phys. Rev.* **D95**, 024010 (2017), [arXiv:1607.05661](https://arxiv.org/abs/1607.05661) [gr-qc].

- [14] S. Ossokine et al., in preparation, 2019.
- [15] M. Breschi, S. Bernuzzi, F. Zappa, M. Agathos, A. Perego, D. Radice, and A. Nagar, *Phys. Rev.* **D100**, 104029 (2019), [arXiv:1908.11418 \[gr-qc\]](#).
- [16] T. Hinderer et al., *Phys. Rev. Lett.* **116**, 181101 (2016), [arXiv:1602.00599 \[gr-qc\]](#).
- [17] J. Steinhoff, T. Hinderer, A. Buonanno, and A. Taracchini, *Phys. Rev.* **D94**, 104028 (2016), [arXiv:1608.01907 \[gr-qc\]](#).
- [18] B. D. Lackey, M. Pürrer, A. Taracchini, and S. Marsat, (2018), [arXiv:1812.08643 \[gr-qc\]](#).
- [19] E. Barausse and A. Buonanno, *Phys.Rev.* **D81**, 084024 (2010), [arXiv:0912.3517 \[gr-qc\]](#).
- [20] E. Barausse, E. Racine, and A. Buonanno, *Phys. Rev.* **D80**, 104025 (2009), [arXiv:0907.4745 \[gr-qc\]](#).
- [21] E. Barausse and A. Buonanno, *Phys.Rev.* **D84**, 104027 (2011), [arXiv:1107.2904 \[gr-qc\]](#).
- [22] A. Taracchini, Y. Pan, A. Buonanno, E. Barausse, M. Boyle, et al., *Phys.Rev.* **D86**, 024011 (2012), [arXiv:1202.0790 \[gr-qc\]](#).
- [23] A. Taracchini, A. Buonanno, Y. Pan, T. Hinderer, M. Boyle, et al., *Phys.Rev.* **D89**, 061502 (2014), [arXiv:1311.2544 \[gr-qc\]](#).
- [24] T. Hinderer et al., *Phys. Rev.* **D88**, 084005 (2013), [arXiv:1309.0544 \[gr-qc\]](#).
- [25] T. Damour and A. Nagar, *Phys.Rev.* **D90**, 044018 (2014), [arXiv:1406.6913 \[gr-qc\]](#).
- [26] A. Nagar, T. Damour, C. Reisswig, and D. Pollney, *Phys. Rev.* **D93**, 044046 (2016), [arXiv:1506.08457 \[gr-qc\]](#).
- [27] A. Nagar, G. Riemenschneider, and G. Pratten, *Phys. Rev.* **D96**, 084045 (2017), [arXiv:1703.06814 \[gr-qc\]](#).
- [28] A. Nagar and P. Rettengo, *Phys. Rev.* **D99**, 021501 (2019), [arXiv:1805.03891 \[gr-qc\]](#).
- [29] S. Akcay, S. Bernuzzi, F. Messina, A. Nagar, N. Ortiz, and P. Rettengo, *Phys. Rev.* **D99**, 044051 (2019), [arXiv:1812.02744 \[gr-qc\]](#).
- [30] T. Damour, P. Jaranowski, and G. Schäfer, *Phys.Rev.* **D78**, 024009 (2008), [arXiv:0803.0915 \[gr-qc\]](#).
- [31] T. Damour, *Phys. Rev.* **D64**, 124013 (2001), [arXiv:gr-qc/0103018](#).
- [32] D. Bini, T. Damour, and A. Geralico, *Phys. Rev.* **D92**, 124058 (2015), [Erratum: *Phys. Rev.* **D93**, no.10, 109902 (2016)], [arXiv:1510.06230 \[gr-qc\]](#).
- [33] S. Akcay, L. Barack, T. Damour, and N. Sago, *Phys. Rev.* **D86**, 104041 (2012), [arXiv:1209.0964 \[gr-qc\]](#).
- [34] A. Nagar, *Phys.Rev.* **D84**, 084028 (2011), [arXiv:1106.4349 \[gr-qc\]](#).
- [35] A. Nagar, G. Pratten, G. Riemenschneider, and R. Gamba, (2019), [arXiv:1904.09550 \[gr-qc\]](#).
- [36] S. E. Field, C. R. Galley, J. S. Hesthaven, J. Kaye, and M. Tiglio, *Phys.Rev.* **X4**, 031006 (2014), [arXiv:1308.3565 \[gr-qc\]](#).
- [37] M. Pürrer, *Class. Quant. Grav.* **31**, 195010 (2014), [arXiv:1402.4146 \[gr-qc\]](#).
- [38] M. Pürrer, *Phys. Rev.* **D93**, 064041 (2016), [arXiv:1512.02248 \[gr-qc\]](#).
- [39] C. R. Galley and P. Schmidt, (2016), [arXiv:1611.07529 \[gr-qc\]](#).
- [40] B. D. Lackey, S. Bernuzzi, C. R. Galley, J. Meidam, and C. Van Den Broeck, *Phys. Rev.* **D95**, 104036 (2017), [arXiv:1610.04742 \[gr-qc\]](#).
- [41] S. Balmelli and T. Damour, *Phys. Rev.* **D92**, 124022 (2015), [arXiv:1509.08135 \[gr-qc\]](#).
- [42] “SXS Gravitational Waveform Database,” <https://data.black-holes.org/waveforms/index.html>.